# cmgh

ORIGINAL RESEARCH

Self-renewing Monolayer of Primary Colonic or Rectal Epithelial Cells

Yuli Wang,[1] Matthew DiSalvo,[2] Dulan B. Gunasekara,[1] Johanna Dutton,[2] Angela Proctor,[1] Michael S. Lebhar,[2] Ian A. Williamson,[2] Jennifer Speer,[1] Riley L. Howard,[3] Nicole M. Smiddy,[1] Scott J. Bultman,[4] Christopher E. Sims,[1] Scott T. Magness,[2] and Nancy L. Allbritton[1,2,3]

[1]Department of Chemistry, University of North Carolina, Chapel Hill, North Carolina; [2]Joint Department of Biomedical Engineering, University of North Carolina, Chapel Hill, and North Carolina State University, Raleigh, North Carolina; and [3]Department of Applied Physical Sciences and [4]Department of Genetics, University of North Carolina, Chapel Hill, North Carolina
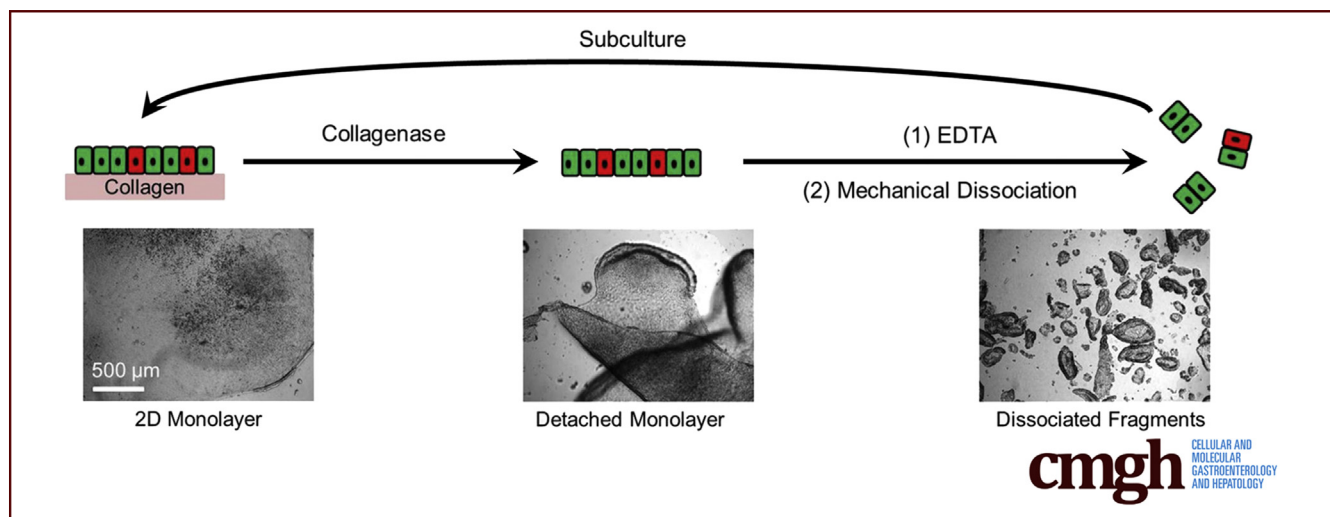
SUMMARY

Self-renewing, 2-dimensional primary colonic epithelial cells are sustained by a combination of surface matrix and chemical factors. The 2-dimensional culture platform is a physiologically relevant system to assay stem cell renewal and differentiation and to screen compounds.

BACKGROUND & AIMS: Three-dimensional organoid culture has fundamentally changed the in vitro study of intestinal biology enabling novel assays; however, its use is limited because of an inaccessible luminal compartment and challenges to data gathering in a three-dimensional hydrogel matrix. Long-lived, self-renewing 2-dimensional (2-D) tissue cultured from primary colon cells has not been accomplished.

METHODS: The surface matrix and chemical factors that sustain 2-D mouse colonic and human rectal epithelial cell monolayers with cell repertoires comparable to that in vivo were identified.

RESULTS: The monolayers formed organoids or colonoids when placed in standard Matrigel culture. As with the colonoids, the monolayers exhibited compartmentalization of proliferative and differentiated cells, with proliferative cells located near the peripheral edges of growing monolayers and differentiated cells predominated in the central regions. Screening of 77 dietary compounds and metabolites revealed altered proliferation or differentiation of the murine colonic epithelium. When exposed to a subset of the compound library, murine organoids exhibited similar responses to that of the monolayer but with differences that were likely attributable to the inaccessible organoid lumen. The response of the human primary epithelium to a compound subset was distinct from that of both the murine primary epithelium and human tumor cells.

CONCLUSIONS: This study demonstrates that a self-renewing 2-D murine and human monolayer derived from primary cells can serve as a physiologically relevant assay system for study of stem cell renewal and differentiation and for compound screening. The platform holds transformative potential for personalized and precision medicine and can be applied to emerging areas of disease modeling and microbiome studies. *(Cell Mol Gastroenterol Hepatol 2017;4:165–182; http://dx.doi.org/10.1016/j.jcmgh.2017.02.011)*

Keywords: Colonic Epithelial Cells; Monolayer; Organoids; Compound Screening.

Long-term culture of primary intestinal epithelial tissue as a planar monolayer has not been possible because of the rapid loss of stem and proliferative cells and rapid onset of apoptosis when primary epithelium is placed into culture.[1] Investigators have traditionally relied on colon cancer cell lines such as Caco-2 and its derivatives to study gut epithelial physiology because of their ability to grow indefinitely on conventional tissue culture plates.[2] Although cancer cell lines grow as confluent monolayers and can be efficiently passaged, they possess many non-physiologic characteristics including somatic mutations, chromosomal instabilities, altered metabolism, and aberrant proliferative and differentiation characteristics.[3] Together, these non-physiologic properties of Caco-2 cells call into question their predictive ability in assays designed to understand normal epithelial physiology.

Recent advances in epithelial culture conditions now promote intestinal stem cell (ISC) maintenance and indefinite culture of primary intestinal tissue as three-dimensional (3-D) organoids.[4–8] The organoid culture system uses soluble growth factors including Wnt-3A, R-spondin, noggin, and epidermal growth factor (EGF) to mimic the ISC niche environment that supports ISC survival, growth, and differentiation in a thick layer of Matrigel.[5,8–10] Like in vivo, organoid ISCs exhibit their defining properties by self-renewing and giving rise to progenitors that differentiate into absorptive colonocytes (water and electrolyte uptake), goblet cells (mucus production), enteroendocrine cells (hormones), and Paneth cells (antimicrobial and stem cell niche functions).[5] By virtue of their non-transformed condition, 3-D organoids represent a physiologically relevant model enabling novel assays and pharmaceutical and dietary compound screens that are not currently possible with colon cancer cell lines such as Caco-2.[3,11,12]

Although organoid culture technology has had a major positive impact on the in vitro study of primary gut epithelium, the 3-D geometry of organoids prevents access to the apical aspect of the epithelium, producing a number of challenges to physiologically relevant studies. The apical surface of the organoid is analogous to the lumen of the gut where digested contents and microbial communities interact with the epithelium. The spheroidal architecture of the organoids prevents access of exogenous compounds to the luminal epithelial surface, limiting studies focused on apical transporters, receptors, metabolic enzymes, and microbiota.[13] Matrigel embedded organoids exist in multiple planes, making collection of experimental readout by using conventional microscopy exceptionally challenging.[14,15] Unfolding the spherical organoid into a two-dimensional (2-D) planar tissue construct is a solution that addresses these major challenges and has the potential to further transform in vitro study of the gut epithelium.

We have previously demonstrated that primary intestinal epithelial cells can be cultured on polydimethylsiloxane (PDMS) and other artificial surfaces in the absence of a hydrogel.[4] Although they are supplied with the requisite soluble growth factors for growth within Matrigel, culture of primary epithelium on non-hydrogel surfaces produced a short-lived, non-proliferative monolayer of cells. Dissociated 3-D small intestinal and colonic organoids have been cultured on a porous membrane (coated with 0.1% gelatin or 10 μg/cm^2 collagen) to form a monolayer, but these monolayers were not self-renewing, suggesting that stem cells were lost from the monolayers over time and a self-renewing ISC compartment was not supported.[16,17] The failure of existing 2-D culture methods to produce long-term monolayers suggests that a biochemical environment composed of media and soluble growth factors alone is not adequate to sustain a self-renewing monolayer containing both stem and differentiated cells. To overcome the limitations in monolayer culture duration, we sought to identify parameters that would support self-sustaining monolayers.

Materials and Methods
Isolation of Crypts From Mouse Colon and Human Rectal Biopsies

Male mice were used at age 6–10 weeks. All experiments were performed in compliance with the relevant laws and institutional guidelines at the University of North Carolina (UNC). All experiments and animal usage were approved by the Institutional Animal Care and Use Committee (IACUC) at UNC. Mice were humanely killed by lethal dose of isoflurane, followed by cervical dislocation under the approved UNC IACUC-approved protocol #13-200. A cytomegalovirus enhancer plus chicken actin promoter (CAG)-DsRed mouse model in which all cells expressed the DsRed fluorescent protein was used to monitor the proliferation of colonic epithelial cells by fluorescence microscopy. CAG-DsRed heterozygous mice were bred on a CD-1 background, and wild-type mice were bred on a C57BL/6 background. Wild-type mice were used for fluorescence-based assays and compound screens. An Lgr5EGFPCreERT2xR26 confetti mouse was used for lineage tracing experiments on the 2-D monolayer. The confetti mouse was injected with 5 mg tamoxifen at 48 hours before death and isolation of crypts from the large intestine.[18] Human rectal biopsies were obtained from UNC Hospitals Meadowmont Endoscopy Center

Ⓐ **Most current article**

with consent of the patient (under the approved UNC Institutional Review Board #14-2013).

Isolation buffer was composed of 5.6 mmol/L Na_2HPO_4 (Sigma S7907; Sigma-Aldrich, St Louis, MO), 8.0 mmol/L KH_2PO_4 (Sigma P5655; Sigma-Aldrich), 96.2 mmol/L NaCl (Sigma S5886; Sigma-Aldrich), 1.6 mmol/L KCl (Sigma P5405; Sigma-Aldrich), 43.4 mmol/L sucrose (Fisher BP220-1; Thermo Fisher Scientific, Waltham, MA), and 54.9 mmol/L D-sorbitol (Fisher BP439-500; Thermo Fisher Scientific) in deionized water. The buffer was filter sterilized and stored at 4°C. Ethylenediamine tetraacetic acid (2 mmol/L; Thermo-Fisher 15575020) and DL-dithiothreitol (0.5 mmol/L; Ther-moFisher R0861) were added to 10 mL isolation buffer and used within 2 hours. Colon tissue was incubated in the above ethylenediamine tetraacetic acid/DL-dithiothreitol solution at room temperature for 75 minutes. The tissue was then rinsed with 5 mL isolation buffer twice and vigorously shaken by hand in 10 mL isolation buffer to release the crypts. The density of crypts in the solution was obtained by adding a 10-μL suspension to a Petri dish and counting the number of crypts in this drop of suspension. Released crypts were placed into culture within 30 minutes of isolation.

Medium Composition

The composition of culture media for primary cells is listed in Supplementary Table 1. For mouse cells, the culture medium (ENR-W) was advanced Dulbecco modified Eagle medium/F12 medium with Wnt-3A (30 ng/mL), R-spondin-2 (75 ng/mL), noggin (71 ng/mL), EGF (50 ng/mL; PeproTech 315-09, Rocky Hill, NJ), N-acetyl cysteine (1 mmol/L, Sigma A9165; Sigma-Aldrich), GlutaMAX ($\times$1), HEPES (10 mmol/L), A83-01 (500 ng/mL, Sigma SML0788), penicillin (100 units/mL), streptomycin (100 μg/mL), and gentamicin (5 μg/mL). For human cells, the human intestinal stem cell medium (HISC) was same as ENR-W, except that Wnt-3A (100 ng/mL), R-spondin-2 (90 ng/mL), N-ace-tylcysteine (1.25 mmol/L) and additional B27 ($\times$1), nicotin-amide (10 mmol/L, Sigma N0636), gastrin (10 nmol/L, AnaSpec AS-64149; Fremont, CA), SB202190 (3 μmol/L, Selleckchem S1077; Houston, TX), and prostaglandin E_2 (10 nmol/L, Cayman Chemicals 14010; Ann Arbor, MI) were added. The reagents without specified vendor name and catalog number were from Thermo Fisher Scientific. Wnt-3A, R-spondin-2, and noggin were obtained from conditioned media as described previously.[19] The concentration of Wnt-3A and R-spondin 2 was measured by using a TCF/LEF luciferase reporter stable HEK293 cell line (Signosis SL-0015; Sunnyvale, CA) with comparison to recombinant Wnt-3A and R-spondin 2 control proteins (R&D Systems 1324-WN, 6946-RS-025/CF; Minneapolis, MN). The activity of noggin was measured by using an enzyme-linked immunosorbent assay kit (LifeSpan BioSciences LS-F5920; Seattle, WA).

Three-dimensional Organoid Culture

Isolated crypts were embedded in Matrigel as described previously.[7,20] Briefly, 10,000 crypts were suspended in 50 μL cold Matrigel (Corning 356235; Corning, NY). A 5-μL crypt suspension was added to each well of a 96-well plate. After solidification of the Matrigel at 37°C for 15 minutes, 150 μL medium was added to each well. The medium was changed every 48 hours. The Y-27632 ROCK inhibitor (10 μmol/L, ApexBio A3008-200; Houston, TX) was added to the medium for the first 48 hours of culture. Every 4 days (mouse cells) or 7 days (human cells), the organoids were dissociated with Accutase (Stemcell Technologies 07920; Vancouver, Canada) and passaged to a new 96-well plate at a ratio of 1:3.

Preparation of the Collagen Hydrogel in Six-well Plate

Collagen hydrogel is generally prepared by neutralizing the acidic collagen solution with NaOH and incubating the mixture at 37°C for 30–60 minutes. The hydrogel properties (eg, stiffness, clarity, adhesiveness, cell-binding sites) are highly dependent on the pH during gelation. Therefore, we used a customized neutralization buffer (containing HEPES, $NaHCO_3$, and NaOH in phosphate-buffered saline [PBS]) to neutralize the acidic collagen solution before gelation to ensure a final pH of 7.4 for the hydrogel. The neutralization buffer was prepared in 75-mL volumes. If the acidic collagen solution has a protein concentration of 4 mg/mL (in 0.02 N-acetic acid), the components necessary for preparation of 75 mL neutralization buffer are the following: $\times$10 PBS (Corning 46-013-CM), 10 mL; HEPES (1 N, ThermoFisher 15630080, pH = 7.4), 2 mL; sodium bicarbonate (7.5% w/v, Corning 25-035-CI, pH = 8), 6 mL; sodium hydroxide (1 N), 575 μL; and deionized water, 56.4 mL.

The buffer was sterile filtered and stored at room temperature until use. The buffer was used for a maximum of 6 months and then replaced. Each batch of collagen stock solution (type I, rat tail, Corning 356236) can have a different concentration of collagen protein. The above recipe uses collagen with a concentration of 4 mg/mL protein. Volumes used must be adjusted if different collagen protein concentrations are used, so that the final concentration of buffered salts in the neutralized collagen hydrogel is HEPES 20 mmol/L, $NaHCO_3$ 53 mmol/L, and PBS $\times$1.

To prepare 1 mL neutralized collagen at a concentration of 1 mg/mL, 750 μL neutralization buffer was first added to a 15-mL conical tube, and the tube was placed on ice. Then 250 μL collagen stock solution (type I, rat tail, Corning 356236, 4 mg/mL, 4°C) was added to the tube, and the mixture was homogenized by slow and repeated pipetting, carefully avoiding air bubble formation during pipetting. The collagen mixture (1 mL) was added to each well of a 6-well plate (Denville T1006; Holliston, MA). The plate was incubated at 37°C for 1 hour to generate a clear hydrogel. PBS (4 mL) was placed over the hydrogel. The collagen hydrogel was gener-ally used within 2 hours after preparation but could be stored in a 37°C incubator up to 1 month without apparent loss of integrity, adhesion, and cell culture outcome. The thickness of the collagen hydrogel was 1 mm in the 6-well plates.

Two-dimensional Monolayer Culture on a Collagen Hydrogel

The crypts were placed on top of the collagen hydrogel at a density of 1000 crypts/cm^2 (unless otherwise stated)

and cultured in 4 mL medium per well in the 6-well plate. The medium was changed every 48 hours, and Y-27632 was added for the initial 48 hours of culture. When the cell coverage was greater than 80% (typically after 3–4 days for mouse cells, 5–7 days for human cells), the monolayers were subcultured by a gentle 2-step dissociation method. The first step was to lift up the monolayer from the collagen hydrogel by scraping the collagen (with cells) from the well and transferring the hydrogel to a 15-mL conical tube containing 1 mL culture medium with 500 U/mL collagenase (type IV, Worthington Biochemical LS004189; Lakewood, NJ). The gel was broken into small pieces by pipetting using a 5-mL serologic pipette, followed by a 1-mL pipet tip. The tube was then incubated at 37°C for 10 minutes to completely digest the collagen gel. The monolayers were rinsed with PBS buffer and pelleted by centrifugation at $600g$ for 1 minute. The second step was to further break up the monolayer pieces into smaller fragments by incubating the pellet in 150 μL ethylenediamine tetraacetic acid (0.5 mmol/L) and Y-27632 (10 μmol/L) in PBS at 37°C for 2 minutes (mouse cells) or 5 minutes (human cells). The monolayers were broken into small fragments by pipetting up and down 30 times by using a 200-μL pipet tip. The cell fragments were resuspended in medium and subcultured on a new collagen hydrogel at a passage ratio of 1:3.

To convert 3-D organoids to a 2-D monolayer, the organoids were extracted from Matrigel by detaching the Matrigel patty, breaking it into coarse pieces, and then pipetting the suspension by using a 200-μL pipet tip. The cells were then cultured on a collagen gel at a density of 10 organoids/cm^2.

Culture on Surfaces Other Than Collagen

When cells were cultured on a Matrigel surface, ie, not embedded, Matrigel at a protein concentration of 8.9 mg/mL was added to each well of a 24-well plate and gelled at 37°C for 1 hour. For polystyrene surfaces coated with different extracellular matrix (ECM) coatings, tissue culture grade polystyrene was coated with ECM or peptides by incubation at 37°C for 1 hour at a concentration recommended by the vendors. Gelatin (10 mg/mL) was prepared by cross-linking with transglutaminase.[21] Polyacrylamide possessed a stiffness of about 800 Pa, and its surface was covalently attached to collagen by sulfosuccinimidyl 6-(4′-azido-2′-nitrophenylamino) hexanoate as recommended by the manufacturer.

Stiffness Measurements

Stiffness measurements were conducted by using a TA Instruments Discovery Hybrid Rheometer (New Castle, DE) (DHR3) in dynamic mechanical analysis mode.

Characterization of the Two-dimensional Monolayer

The proliferation and viability of cells were quantified by either surface area coverage or a cell viability assay (CellTiter-Glo luminescence assay, Promega G7572; Madison, WI). To ensure the cells possessed grossly normal chromosomes, cells were karyotyped (KaryoLogic, Inc, Morrisville, NC). Twenty cells from each sample were analyzed. To reveal the topographic features of 2-D monolayer, the samples were dried with a critical point dryer (Tousimis Semidri PVT-3; Rockville, MD) and inspected by scanning electron microscope (SEM) (FEI Quanta 200 ESEM; FEI Company, Hillsboro, OR). For immunofluorescence staining, thin sections (8–10 μm) of the 2-D monolayers were prepared on a cryostat.

Staining and Imaging

5-Ethynyl-2-deoxyuridine staining. The 5-ethynyl-2-deoxyuridine (EDU)-based staining was used to reveal proliferative cells.[22] Cells were incubated with EDU (10 μmol/L) in medium for 3 hours at 37°C, followed by standard staining (Click-iT EDU Alexa Fluor 647 imaging kit; Thermo Fisher Scientific). The cells were imaged by using a Nikon Eclipse TE300 inverted epifluorescence microscope (Chroma ET-Cy5 49006 filter set).

Alkaline phosphatase staining. Alkaline phosphatase (ALP) was used to reveal cells differentiated toward the colonocyte lineage. The live cells were first rinsed with PBS and then incubated for 30 minutes at 37°C with an ALP substrate (Vector red alkaline phosphatase substrate kit; Vector Laboratories, Burlingame, CA) in Tris buffer (0.15 mol/L, pH 8.4). The cells were rinsed with PBS and fixed in 4% paraformaldehyde for 15 minutes. The ALP staining was imaged by brightfield or epifluorescence microscopy (Semrock TxRed-4040B; Rochester, NY).

Other fluorescence staining. Immunofluorescence staining was used to reveal the differentiated phenotypes or subcellular structures. Antibodies against SOX9 (α-Sox9) stain proliferative progenitor and stem cells. Anti-Mucin2 (α-Muc2) marks goblet cells. Anti-chromogranin A (α-ChgA) identifies enteroendocrine cells. Anti–β-catenin, ZO-1, occludin, and E-cadherin labeled cell-to-cell junctions. Anti–integrin-β4 and NA$^+$/K$^+$-ATPase labeled the basal and basolateral membranes. Villin and phalloidin stained the apical surface. For most antibodies, the cells were first fixed with 4% paraformaldehyde for 15 minutes, followed by incubation with 0.5% Triton X-100 for 20 minutes. For ZO-1, E-cadherin, and occludin, the cells were fixed with ice cold methanol and placed at −20°C for 15 minutes. The cells were blocked with 10% donkey serum (Jackson Immunoresearch 017-000-121; West Grove, PA) for 1 hour at 20°C. The cells were incubated in primary antibody at 4°C overnight and stained with a secondary antibody for 45 minutes at 20°C. Finally, the DNA was stained with Hoechst 33342 (2 μg/mL; Sigma-Aldrich, #B2261) for 15 minutes at 20°C. Primary antibodies were rabbit α-Muc2 (1:200, Santa Cruz sc-15334; Santa Cruz Technology, Santa Cruz, CA),[23] rabbit α-ChgA (1:1000, Abcam ab15160; Cambridge, UK),[24] rabbit α-Sox9 (1:100, Millipore AB5535; Billerica, MA),[23] rabbit α-villin (1:200, Santa Cruz sc-28283), rabbit α-ZO-1 (1:100, Proteintech 21773-1-AP; Wuhan, China), rabbit α-E-cadherin (1:100, Proteintech 20874-1-AP), rabbit α-occludin (1:100,

Proteintech 13409-1-AP), rabbit α-NA$^+$/K$^+$-ATPase (1:100, Proteintech 22338-1-AP), rabbit α-integrin-β4 (1:200, Santa Cruz sc-9090), and rabbit α-β-catenin (1:200, Santa Cruz sc-7199).[25] The secondary antibodies were donkey anti-rabbit immunoglobulin G conjugated with either Alexa Fluor 488 or 594 (1:500, Jackson Immunoresearch 711-545-152 or 711-585-152). Alexa Fluor 488 phalloidin (Thermo Fisher A12379) bound to actin.

High-throughput Screening of Dietary Metabolites and Natural Products

All 77 compounds were obtained from Sigma-Aldrich. The names, categories, and their working concentration are listed in Supplementary Table 2. Seventy-five μL collagen hydrogel was prepared in each well of 96-well plates (Corning #3603) by the protocol described above. Fragments of primary mouse colonic epithelial cells (75,000 cells per well) were cultured on the collagen hydrogel with 200 μL ENR-W (with "W" indicating a normal [Wnt-3A] of 30 ng/mL). At 24 hours, the medium was aspirated, and the cells were cultured in medium (200 μL) containing a dietary/natural compound in ENR-w (with "w" indicating a reduced [Wnt-3A] of 10 ng/mL) for an additional 48 hours. The decreased Wnt-3A concentration reduced the Wnt-3A signaling strength, enabling cells to undergo differentiation in response to exogenous compounds. The cells were pulsed with EDU (3 hours), stained for ALP (30 minutes), and then fixed with 4% paraformaldehyde (15 minutes). The cells were then sequentially labeled with the Click-iT EDU reagent, α-Muc2 (Mucin2) and Hoechst 33342. Finally, the cells were thoroughly rinsed with PBS to remove excess reagents. Three 96-well plates were used for each experiment.

Assaying for Hit Dietary Compounds on Mouse Three-dimensional Organoids and Human Two-dimensional Monolayers

Fourteen selected hit compounds were tested on 3-D mouse colonic organoids. Fragments of mouse colonic epithelial cells (25,000 cells per well) were embedded in 4 μL Matrigel in each well of a 96-well plate and cultured with ENR-W (200 μL). At 24 hours, the medium was aspirated, and the cells were cultured in ENR-w (200 μL) containing a dietary/natural compound for an additional 48 hours. Seven selected hit compounds were tested on human rectal 2-D monolayers. Fragments of human rectal epithelial cells (75,000 cells per well) were cultured on the collagen hydrogel in a 96-well plate with HISC medium with high [Wnt-3A] of 100 ng/mL. At 48 hours, the medium was aspirated, and the cells were cultured in medium (200 μL) containing a dietary/natural compound in HISC medium with reduced [Wnt-3A] of 30 ng/mL for an additional 96 hours. The cells were then stained with ALP, EDU, α-Muc2, and Hoechst 33342 in the same manner as the mouse 2-D monolayers described above.

Caco-2 Cells

Caco-2 cells were obtained from UNC Lineberger Comprehensive Cancer Center. The cells were authenticated at the Duke University DNA analysis facility human cell line authentication service by analyzing DNA for polymorphic short tandem repeat markers. Results indicated that "the major STR peaks matched the ATCC reference but the sample also had several outlier peaks not present in either the negative or positive controls." Caco-2 cells (passage number 37) were cultured in a 96-well plate at 28,750 cells per well in Dulbecco modified Eagle medium supplemented with 10% fetal bovine serum, 100 U/mL penicillin, and 100 μg/mL streptomycin. After 24 hours, the cells were incubated in the above medium with the added dietary/natural compound for an additional 48 hours. The Caco-2 cells were then stained with ALP, EDU, α-Muc2, and Hoechst 33342 in the same manner as the primary colonic epithelial cells.

Image Acquisition

After staining, each 96-well plate was imaged by using an Olympus IX81 epifluorescence microscope ($\times$4 objective, N.A. of 0.13, Olympus UPlanFL N; Tokyo, Japan). The imaging area consisted of a grid of either 4 $\times$ 3 or 6 $\times$ 4 overlapping images covering 47%–54% of the total well area. Well-focused images covering the entire image area were obtained by autofocusing on each image position by using a custom script written in MatLab (Natick, MA). Each sample was imaged by using blue, red, far red, and green filter sets (Chroma ET-DAPI 49000, Semrock TxRed-4040B, Chroma ET-Cy5 49006, and Semrock FITC-3540B, corresponding to the Hoechst 33342, ALP, EDU, and Muc2 stains, respectively) and an exposure time of 150 milliseconds for all channels. The total image acquisition time for a 96-well plate using a 6 $\times$ 4 image grid for each well was 456 $\pm$ 7.5 minutes.

Image Analysis

After cropping out the overlapping regions in the image data, the collected images obtained from each well were filtered by using a Wiener filter with a 3 $\times$ 3 pixel neighborhood to reduce noise. The image background was subtracted by using top-hat filtering, and then the images were empirically thresholded. Objects less than 3.1 μm in diameter were removed to eliminate cellular debris and artifacts produced by camera noise. The integrated raw fluorescence intensity over the area occupied by the suprathreshold fluorescence was summed for all images of a sample and for each fluorescence emission wavelength. This summed fluorescence area was then normalized by the total cell area occupied by the Hoechst 33342 fluorescence and plotted against the compound number.

Hit Selection

In high-throughput screens it is important to assess how much the test compounds and negative controls differ from one another. Strictly standardized mean difference (SSMD) was used to quantify the differences between dietary compounds and negative controls.[26] SSMD is commonly used statistic in compound screens and is

calculated as the mean difference between the test sample and reference sample divided by the standard deviation of the difference between the test and reference. SSMD essentially measures effect size for the comparison of 2 groups. Sample #78 was used as the negative reference for SSMD calculations for all tissue types. Compound effects were classified by using standard SSMD thresholds[27]: $|SSMD| \geq 5$ for extremely strong, $5 > |SSMD| \geq 3$ for very strong, $3 > |SSMD| \geq 2$ for strong, $2 > |SSMD| \geq 1.645$ for fairly strong, $1.645 > |SSMD| \geq 1.28$ for moderate, $1.28 > |SSMD| \geq 1$ for fairly moderate, $1 > |SSMD| \geq 0.75$ for fairly weak, $0.75 > |SSMD| \geq 0.5$ for weak, $0.5 > |SSMD| \geq 0.25$ for very weak, and $|SSMD| \leq 0.25$ for extremely weak effects. Compounds with fairly strong or stronger effects on nuclear coverage, ALP signal, or EDU signal were designated hits. Compounds with only fairly moderate or stronger effects on Muc2 signal were designated hits because of the weaker effects apparent across all Muc2 screens. Library screens were performed in triplicate across well plates (mouse and Caco-2 monolayers). The SSMD size effect was calculated by using the paired uniformly minimal variance unbiased estimate of SSMD.[28] For library screens performed in triplicate within single-well plates (human 2-D monolayers and mouse 3-D organoids), the SSMD size effect was calculated by using the unpaired SSMD under unequal variance.[28]

Other Statistics/Methods

Unless otherwise specified, the data shown for each experiment used crypts or cells obtained from a single mouse or 1 human biopsy. All data used 3 technical replicates (n = 3), and the mean with a single standard deviation is shown unless otherwise specified. When the fate of a crypt was assayed, n = 3 wells with 10 crypts/well were counted. Multiple experiments from different mice for all data (except the dietary compound screen) were performed, and the results were consistent over time without outliers. Although the data of each experiment represent those of a single mouse (to reduce animal usage), more than 30 mice were used throughout the work, with no observable difference in monolayer formation or growth rate. This translates into more than 30 different cell lines, but each typically was used for no more than 5 passages to avoid any possibility of chromosomal aberrations. Animals from 2 different backgrounds were used, CD-1 background (CAG-DsRed mice) and C57BL/6 background (Lgr5EGFP-CreERT2xR26 and wild-type mice). Data from representative experiments are presented. Biopsies from 3 different humans were used to develop the human monolayer system. The biopsies were obtained sequentially, with the first 2 biopsies used to optimize the conditions for human cell culture. The data in the article are from the third biopsy specimen. No difference was observed in the properties of the cells from the different biopsies, and the optimized conditions for the first 2 biopsy cells worked well for the third specimen.

All authors had access to the study data and reviewed and approved the final manuscript.

Results

### A Murine Colonic Epithelial Monolayer Proliferates on the Surface of a Collagen Hydrogel

Intestinal stem cells can be maintained as a proliferative culture by providing a medium rich in growth factors and embedding the cells within Matrigel to form 3-D organoids.[7] We hypothesized that a 2-D monolayer of epithelial cells would undergo long-term proliferation if provided with the appropriate matrix cues such as a suitable stiffness in addition to the required soluble factors (Figure 1A and B). Matrigel is widely used in 3-D stem cell culture systems because it resembles the ECM found in many tissues.[7] Crypts cultured on the surface of Matrigel failed to form a spreading 2-D monolayer (Figure 1C). Instead the crypts grew into 3-D organoids residing above the surface (100% ± 0% of crypts, 100 crypts counted per well, n = 3) and possessed morphologies reminiscent of the organoids formed within a Matrigel patty, suggesting that Matrigel did not possess the ECM contacts and stiffness (Young's modulus $\sim$ 50 Pa[29]) required to allow cells to spread on the surface (Figure 1B).

Polystyrene is the most commonly used 2-D cell culture substrate,[31] and polydimethylsiloxane (PDMS) is a dominant material in building cell-based lab-on-chip and microfluidic devices.[32] Crypts plated on a plasma-oxidized polystyrene or PDMS formed an adherent 2-D monolayer, but the cells were short-lived and without evidence of self-renewal (Figure 1C). Similar outcomes were also observed for crypts plated on gelatin, agarose, and polyacrylamide (Figure 1G–iii).

The common practice of coating surfaces with ECM proteins or peptides (Matrigel, collagen, laminin, fibronectin, gelatin, vitronectin, or poly-D-lysine) on plasma-oxidized polystyrene or PDMS did not improve the proliferative capability or viability of cells (Figure 1G–i, ii), suggesting these materials lacked the appropriate stiffness (Young's modulus of PDMS = 0.8–4 MPa,[33] polystyrene = 3–3.5 GPa[34]) or other biophysical and biochemical properties that promote a self-sustaining monolayer.

Collagen hydrogels are widely used matrices for cell culture.[35] After crypts were plated on the surface of collagen hydrogel (type I, rat tail, 1 mg/mL, 1-mm thickness), 93% ± 6% crypts (n = 100 crypts/well, 3 wells) formed a surface-attached monolayer that expanded in area and cell number over time (Figure 1C). Lower concentrations of collagen or collagen/Matrigel composites did not support monolayer formation (Figure 1D–F), possibly because of an inappropriate stiffness and ECM properties. Collagenase was highly effective at release cells from the collagen surface before mechanical dissociation and subculture (Figure 2A and B). Karyotyping demonstrated that cells retained the appropriate number of chromosomes through passage number 5 (Figure 2C). Monolayers grew to sizes >2 mm in diameter (Figure 2B) and were maintained in monolayer form for up to 10 months (the longest time tested).

Monolayers were subjected to a number of morphologic and protein expression analyses to characterize key epithelial properties found in vivo. When examined by electron microscopy, the cells of the self-sustaining
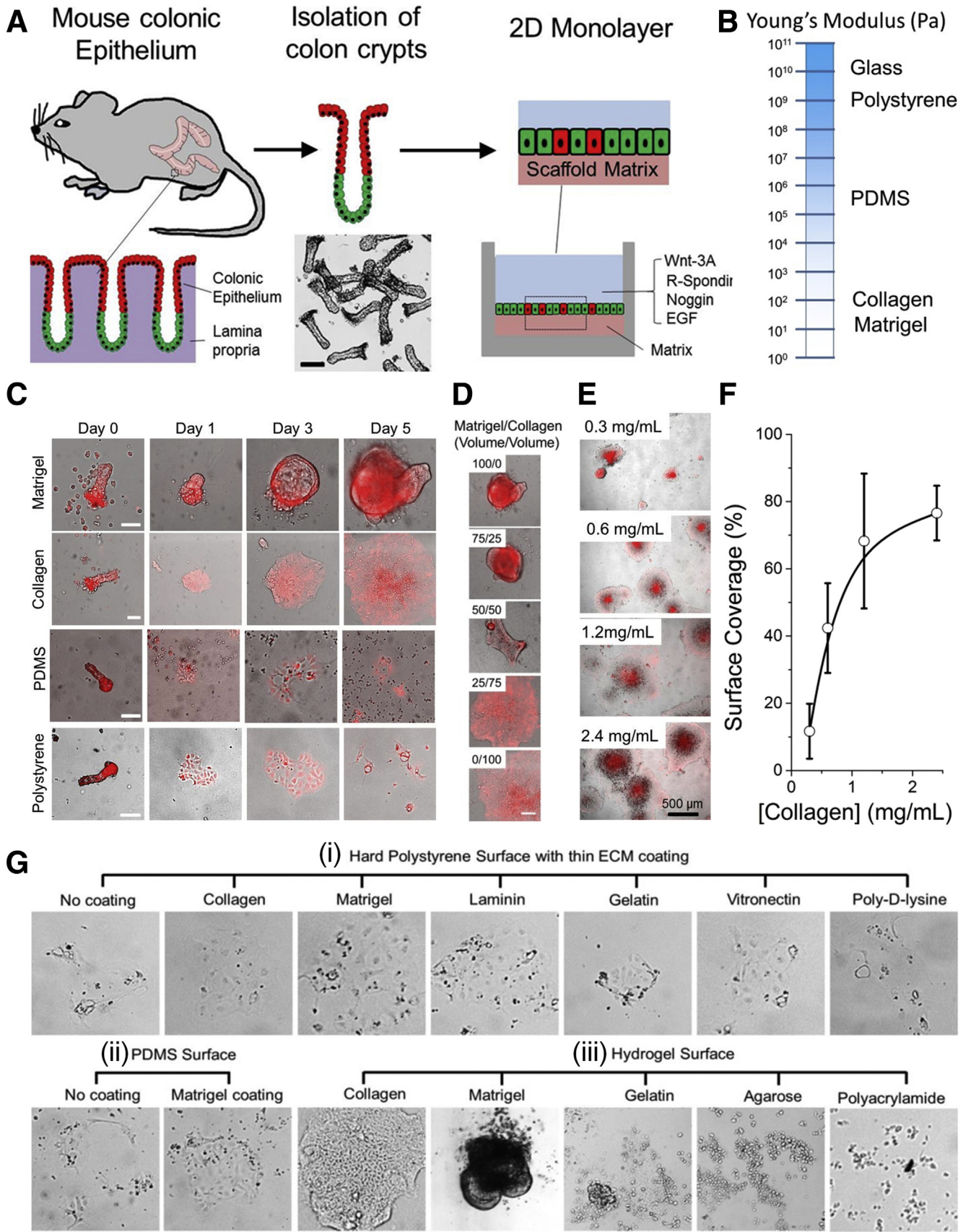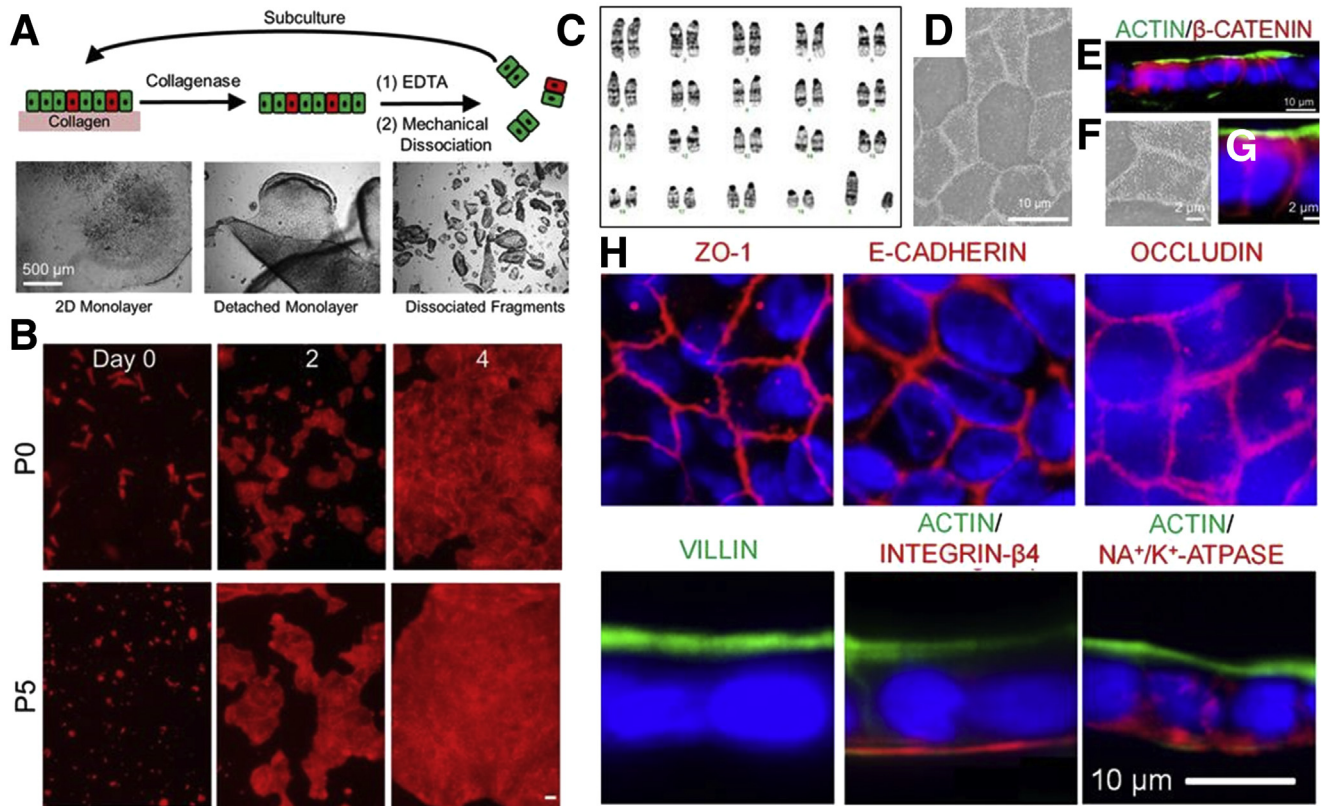
Figure 2. Growth of proliferative 2D monolayer of murine epithelium on surface of collagen hydrogel. (A) Workflow for subculturing 2-D monolayers. Monolayers are dissociated from collagen and split. Brightfield images (*bottom*) show cell preparation at different workflow stages. (B) Time lapse fluorescence (DsRed) images of crypt-derived cells on collagen at passage number 0 (P0, crypts) and passage number 5 (P5). Scale bar $=100$ μm. (C) Karyotype analysis of 2-D monolayer at passage number 5 showing a normal karyotype. (D) SEM image of monolayer on collagen gel at day 3 of culture. (E) Fluorescence image of cross section through the monolayer immunostained for actin (*green*) and β-catenin (*red*). Distribution of β-catenin (an intracellular protein) demonstrated columnar-shaped cells with height of 9.4 ± 0.8 μm and width of 7.5 ± 0.9 μm (n = 10). (F) High magnification view of subregion of (D). (G) High magnification view of subregion of (E). (H) Staining for ZO-1, E-cadherin, or occludin *(red)*; villin or actin *(green)*; integrin-β4 and NA$^+$/K$^+$-ATPase *(red)*. Nuclei *(blue)*.

monolayers demonstrated the hallmark cobblestone arrangement of colonic epithelium (Figure 2D). In vivo, large numbers of microvilli cover the surface of the differentiated colonocytes and function to increase surface area for water and salt absorption. On the monolayers, the microvilli density on each cell was variable, suggesting that cells might be at different states of differentiation (Figure 2D and F). High densities of actin and villin, which are concentrated within microvilli, were present only on the upper or apical cell surface (Figure 2E, G, and H). In contrast, integrin-β4 and NA$^+$/K$^+$-ATPase were localized to the basal and basolateral cell surfaces, respectively,

Figure 1. (*See previous page*). **The 2-D monolayer culture of murine colonic crypts on surface of variety of substrates with different surface properties and stiffness.** (A) Workflow for culturing crypts on matrix surface. Wnt-3A, R-spondin, noggin, and EGF are used in the culture medium. Proliferative stem cells and progenitors *(green);* differentiated cells *(red).* (B) Spectrum of Young's modulus of typical materials used in cell culture. Young's modulus of collagen hydrogel is in the range of 10–1000 Pa,[30] depending on source, type, and concentration of collagen and characterization method. (C) Time-lapse images of crypts cultured on top of 4 matrices with different stiffness: Matrigel (*top panel*), collagen (100 vol%, *second panel*), PDMS (*third panel*), and polystyrene (*bottom panel*). Shown are overlaid brightfield and DsRed fluorescence images. Crypts were derived from a mouse expressing DsRed in all cells under a chicken-actin promoter. Mouse colon crypts were plated on the surfaces at low density of 1 crypt/cm^2 (to track growth of individual crypts) cultured for 5 days. None of the crypts on PDMS and polystyrene formed an expanding monolayer (n = 3 wells, 10 crypts/well). (D) Overlaid brightfield and DsRed images of mouse colonic crypts (CAG-DsRed mouse) cultured on top of mixture of Matrigel/collagen at day 5. (E) Brightfield images of primary mouse colonic epithelial cells cultured for 3 days on surface of collagen hydrogel prepared at 4 concentrations (0.3, 0.6, 1.2, and 2.4 mg/mL). (F) Surface coverage of cells is plotted against concentration of the hydrogel by using data from (E). (G) Culture of mouse colonic crypts on variety of substrates with or without surface coatings. (*i*) Hard polystyrene surface with different ECM coatings. (*ii*) PDMS with and without Matrigel coating. (*iii*) Various hydrogels. Cells proliferated only on collagen and Matrigel. Scale bar = 100 μm unless denoted otherwise.

demonstrating that the cells are polarized with the luminal surface exposed to the medium and the basal surface facing the collagen (Figure 2*H*). Adherens and tight junctions were present between the cells of the monolayer as demonstrated by the localized ZO-1, E-cadherin, and occludin staining (Figure 2*H*). These results suggested that the collagen hydrogel supported epithelial monolayer development closely mimicking that in vivo and also suggest that porosity, ECM proteins, and stiffness of the collagen hydrogel functionally recapitulated key properties of the native colonic basement membrane.

Equivalency of Murine Colonic Two-dimensional Monolayers to Three-dimensional Organoids

Intestinal and colonic organoids embedded within Matrigel possess proliferative and differentiated cellular compartments and are widely accepted as an in vitro tissue model for the digestive tract.[8] Therefore we sought to compare proliferative capacity and lineage composition between the murine 2-D monolayer and 3-D organoid platforms. Colonic crypts were cultured in 3-D (embedded inside Matrigel patty) to form organoids and in 2-D (on the surface of a collagen hydrogel) to form epithelial monolayers (Figure 3*A*). Cell populations in both culture systems rapidly expanded with the monolayer and organoid cells, demonstrating average doubling times of 23.7 hours (95% confidence interval [CI] bounds of 21.3 hours and 26.7 hours, n = 4 technical replicates) and 31.2 hours (95% CI bounds of 25.1 hours and 41.0 hours), respectively (Figure 3*B* and *C*). We observed S-phase cells (EDU$^+$) at day 3 in both 3-D organoids and 2-D monolayers demonstrating actively proliferating cells, suggesting the presence of stem and progenitor cell lineages (Figure 3*D* and *E*). The numbers of organoids and monolayer patches with differentiated cell types (Muc2$^+$ [goblet cells] and ChgA$^+$ [enteroendocrine cells]) were also equivalent in the 2 culture systems, suggesting that the 3-D and 2-D platforms are functionally similar with respect to differentiated secretory lineages (Figure 3*D* and *E*). Cells derived from dissociated monolayers were capable of generating organoids when placed into 3-D culture conditions. Similarly, crypt-derived organoids could be removed from 3-D culture and cultured on the surface of a collagen hydrogel to form a 2-D epithelial monolayer (Figure 3*G* and *H*). There was no distinguishable difference between monolayers derived from freshly isolated crypts or from 3-D cultured organoids. Serial interconversion between the monolayer and organoid morphologies was possible for at least 5 passages (the greatest number tested), indicating that colonic stem cells are maintained in the monolayer (Figure 3*I* and *J*). These data demonstrate that a proliferative monolayer can be derived from multiple sources (crypts, 3-D organoids, and 2-D monolayer fragments).

Mature organoids self-pattern into proliferative and differentiated zones by segregating a high density of stem and progenitor cells to the crypt buds (Figure 3*F*).[36] Although stem cells are self-renewing and persist in the organoid crypt buds, differentiated cells in the organoid have a limited life span and are eventually sloughed into the central pseudolumen. Spontaneous patterning of proliferative and differentiated cellular compartments was also observed within the monolayers after 8 days in culture (Figure 3*F*). Proliferative cells (EDU$^+$) were enriched along the edges of the expanding monolayer, whereas differentiated cells such as goblet cells were concentrated in the center of the monolayer. These data demonstrate that monolayer and organoid culture systems readily interconvert and are equivalent in terms of the cell proliferative capacity, lineage composition, and spontaneous compartmentalization of stem/proliferative cells and differentiated cells.

Lineage Tracing Confirms the Presence of Stem Cells in the Murine Two-dimensional Monolayer

To determine whether self-renewing colonic stem cells persisted in the 2-D monolayers, we performed lineage tracing by using the Lgr5EGFPCreERT2xR26 transgenic mouse. Colonic crypts were isolated from a tamoxifen-treated Lgr5EGFPCreERT2xR26 confetti mouse and plated on the surface of collagen hydrogel at a low density of 30 crypts/cm^2 (to track the growth of individual crypts). At 24 hours after plating, tracing events (4 out of 3000 crypts) expressed red fluorescent protein (RFP), which marked them as derived from Lgr5 stem cells (Figure 4*A*). The RFP$^+$ regions expanded into large red fluorescent patches intermixed with the progeny of non-fluorescent stem cells. RFP$^+$ cells were isolated from 2-D patches and subcultured to determine whether the RFP$^+$ patches contained cells with colonic stem cell properties. The RFP$^+$ cells continued to expand into patches composed only of RFP$^+$ cells (Figure 4*B*). The RFP$^+$ cell monolayers possessed proliferative (EDU$^+$) cells and the differentiated cell types: goblet cells (Muc2$^+$), enteroendocrine cells (ChgA$^+$), and absorptive colonocytes (ALP$^+$) (Figure 4*C*). These data demonstrate that the 2-D monolayers possessed Lgr5 ISCs that expanded as a proliferative monolayer and produced differentiated descendants in vitro.

Human Rectal Epithelial Cells Form Proliferative Two-dimensional Monolayers

To determine whether human rectal epithelial cells might form a proliferative monolayer, human rectal crypts obtained from rectal biopsies were cultured on collagen hydrogel in medium with the appropriate growth factors. Eighty-five percent ± 5% crypts (n = 3, 20 crypts monitored per experiment) formed a monolayer that expanded in area over time (Figure 5*A*). The cells were subcultured every 5–7 days and maintained as a monolayer. The human 2-D monolayer and 3-D organoids could be interconverted without loss of proliferative capability (Figure 5*B* and *C*). Similar to 3-D organoid culture, the cells remained proliferative, with cell number increasing over time (Figure 5*D*). The doubling times measured during log-linear cell growth were 46.5 hours (95% CI bounds of 39.4 hours and 56.6 hours) for 2-D monolayer and 47.1 hours (95% CI bounds of 40.8 hours and 55.8 hours) for 3-D organoids. The human cells demonstrated a normal karyotype at passage number 6
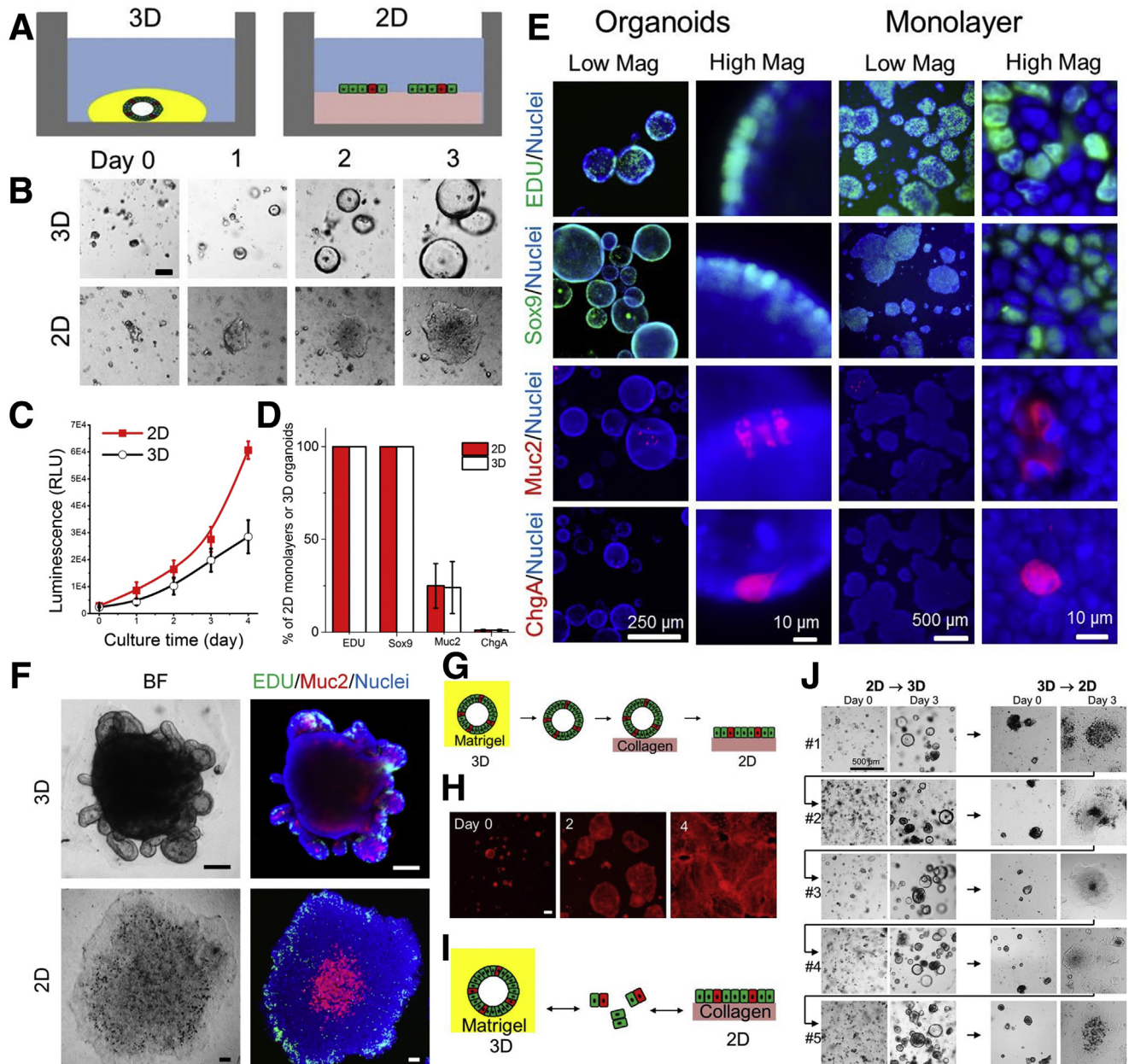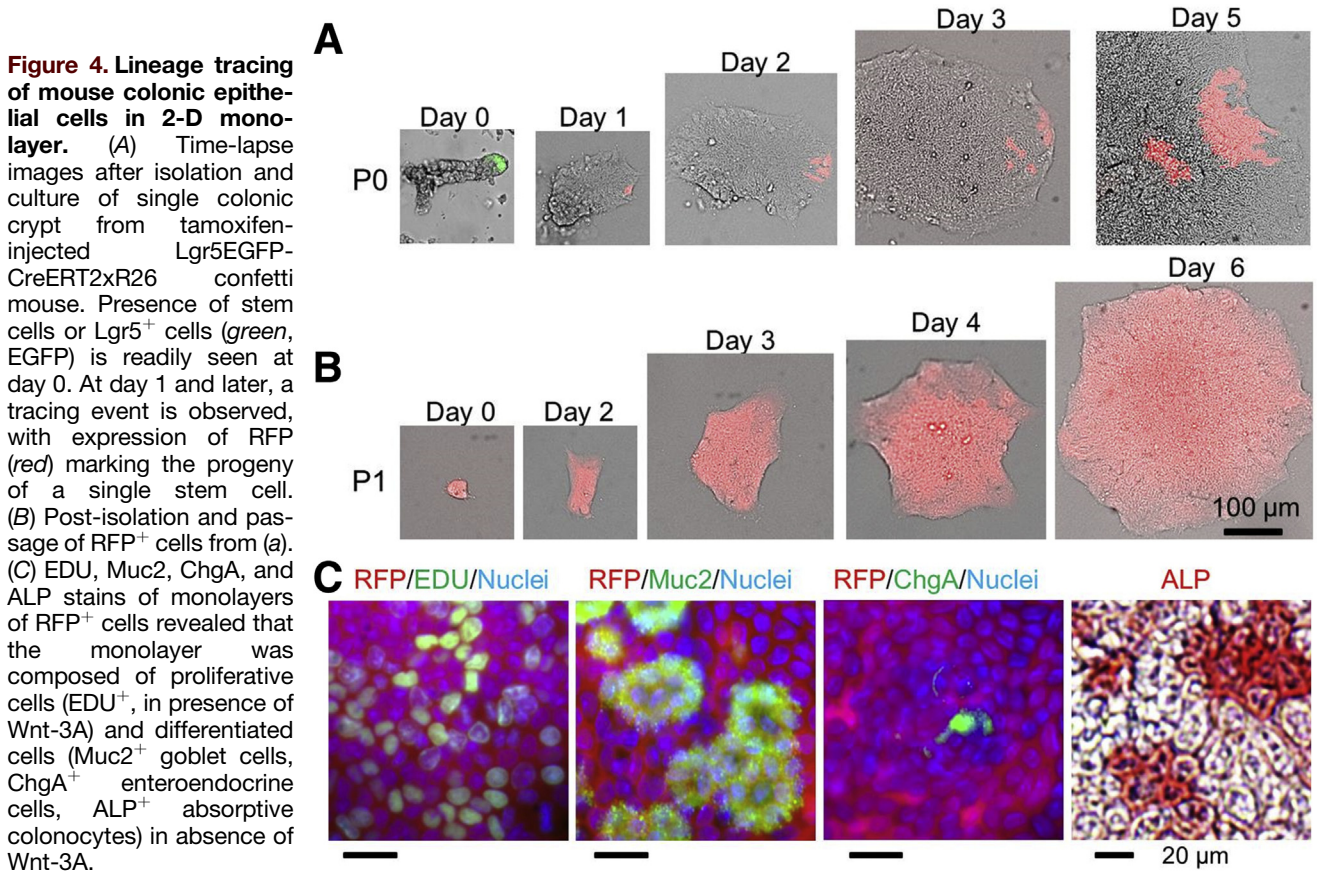
Figure 3. Proliferative capacity, lineage composition, and compartmentalization are highly similar between 2-D murine colonic monolayers and 3-D organoids. (*A*) Schematic showing culture format for organoids and monolayers. (*B*) Time-lapse brightfield images demonstrating growth and morphology of crypt-derived organoids and monolayers at passage number 2 (P2). (*C*) Quantification of cellular growth over time in organoids and monolayers measured by proxy assay (CellTiter-Glo luminescence, n = 4). (*D*) Percentage of monolayer patches and organoids at day 3 demonstrating positive staining for proliferative and differentiated cell lineages (EDU, SOX9, Muc2, and ChgA; n = 3, 20 monolayer patches or organoids per experiment). (*E*) Fluorescence images of organoids and monolayers at day 3 (EDU [*green*], SOX9 [*green*], Muc2 [*red*], ChgA [*red*], and nuclei [*blue*]). (*F*) Compartmentalization of proliferative stem/progenitor cells and differentiated cells. Brightfield (*left column*) and fluorescence (*right column*) images of organoids (*top row*) and monolayers (*bottom row*) at culture day 8 (EDU [*green*], Muc2 [*red*], and nuclei [*blue*]). Of the 3-D mature organoids, 80% ± 10% (10 organoids/well, n = 3 wells) demonstrated increased stem/progenitors (EDU$^+$) collections in the buds, whereas 100% ± 0% (10 monolayer patches/well, n = 3 wells) of the monolayers demonstrated EDU$^+$ cells localized to periphery of the patch. In a majority (83% ± 6%, 10 monolayer patches/well, n = 3 wells) of monolayer patches, Muc2$^+$ was found only in central-most region of the patch. Mucin was present in the lumen of all 3-D organoids. (*G*) Schematic showing conversion of 3-D organoids into 2-D monolayers. (*H*) DsRed fluorescence images of organoid placement and culture on collagen hydrogel at days 0, 2, and 4. The organoid spreads on the surface to become a cell monolayer. (*I*) Schematic of interconversion of organoids and monolayers performed in panel (*J*). (*J*) Representative images of 5 sequential, interconverting passages from 2-D monolayer to 3-D organoid and back again. Unlike 3-D organoids with enclosed lumen, the epithelial monolayer on collagen possessed an accessible luminal surface. Scale bar = 100 μm unless denoted otherwise.

Figure 4. Lineage tracing of mouse colonic epithelial cells in 2-D monolayer. (*A*) Time-lapse images after isolation and culture of single colonic crypt from tamoxifen-injected Lgr5EGFP-CreERT2xR26 confetti mouse. Presence of stem cells or Lgr5$^+$ cells (*green*, EGFP) is readily seen at day 0. At day 1 and later, a tracing event is observed, with expression of RFP (*red*) marking the progeny of a single stem cell. (*B*) Post-isolation and passage of RFP$^+$ cells from (*a*). (*C*) EDU, Muc2, ChgA, and ALP stains of monolayers of RFP$^+$ cells revealed that the monolayer was composed of proliferative cells (EDU$^+$, in presence of Wnt-3A) and differentiated cells (Muc2$^+$ goblet cells, ChgA$^+$ enteroendocrine cells, ALP$^+$ absorptive colonocytes) in absence of Wnt-3A.

(Figure 5*F*). When examined by electron microscopy, the apical surface of the 2-D monolayer demonstrated microvilli at varying density, suggesting the presence of cells of absorptive colonocyte lineage because microvilli are a hallmark of these absorptive cells (Figure 5*E*). At day 3 in culture, all 3-D organoids and 2-D monolayer patches possessed actively proliferating cells (EDU$^+$ and SOX9$^+$), suggesting the presence of stem and progenitor cell lineages (Figure 5*G* and *H*).[23,36,37] Goblet cells (Muc2$^+$) and enteroendocrine cells (ChgA$^+$) were observed in both human 3-D organoids and 2-D monolayers at day 6 in culture, indicating the presence of differentiated cells (Figure 5*G* and *H*). Cells in the 2-D monolayer possessed β-catenin at the intercellular borders, suggesting the formation of tight intercellular connections (Figure 5*H*). The cells also demonstrated appropriate polarity with actin and integrin-β4 localized to their apical and basal surfaces, respectively (Figure 5*H*). These data demonstrate that the collagen hydrogel system supports the proliferation of human rectal epithelial cells as a 2-D monolayer.

Screening Dietary Components and Food Metabolites on Murine Colonic Monolayers Reveals Specific Impacts on Cell Proliferation and Differentiation

Sustainable 2-D monolayers derived from primary tissue represent a transformative technology for personalized and precision medicine applications that rely on drug and compound screening. Critical for high-throughput screening platforms is the flat, accessible luminal surface of the monolayer, permitting cell interrogation with conventional assays and instrumentation including high-content microscopy.

To demonstrate the utility of the 2-D murine colonic monolayers, 77 naturally occurring compounds found in food and metabolites of digestion were assayed for their ability to alter proliferation and differentiation, attributes that are central to intestinal barrier function and repair in the face of repeated chemical, physical, immune, and infectious insults. The 77 compounds represented a range of chemical classes with diverse or unknown impact on primary intestinal cells and included bioactive food components and metabolites such as fatty acids, bile acids, flavonoids, phytoestrogens, phenols, terpenoids, nitrates, and others (Supplementary Table 2).

Monolayers were grown for 24 hours under normal Wnt-3A concentration of 30 ng/mL (ENR-W), followed by incubation with the dietary/natural compounds in a reduced Wnt-3A concentration of 10 ng/mL (ENR-w) for 48 hours. Decreased Wnt-3A in the medium was used to bring the levels of Wnt signaling to a threshold that would make pro-proliferative or pro-differentiation effects of the compounds readily apparent. After exposing 2-D monolayers to exogenous compounds, the monolayers were sequentially
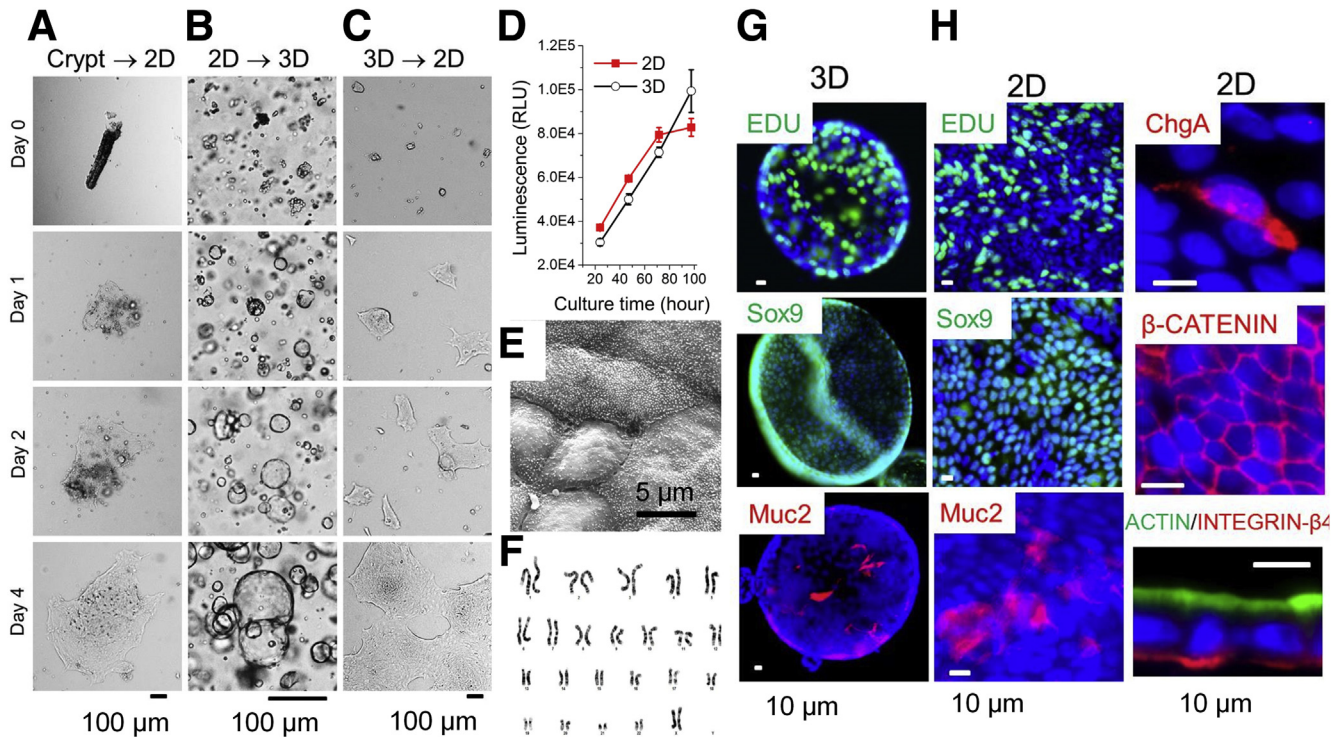
Figure 5. Human rectal epithelial cells can be cultured as proliferative 2-D monolayer. (A) Crypt cultured on top of collagen hydrogel grew as 2-D monolayer. (B) Conversion of fragments of 2-D monolayer to 3-D organoids. The 3-D organoids possessed a thin wall and cystic structure. (C) Conversion of 3-D organoids to 2-D monolayer. The 3-D organoids were extracted from Matrigel (day 4 in culture) and plated on top of collagen hydrogel. (D) Cellular growth over time in organoids and monolayers measured by cell viability assay (CellTiter-Glo luminescence, n = 3). (E) SEM image of monolayer on collagen hydrogel at day 3 of culture. (F) Karyotype analysis of 2-D monolayer at passage 6 showing normal karyotype. (G) Fluorescence images of organoids showing EDU staining (green, at day 3), Sox9 (green, at day3), and Muc2 (red, at day 6) immunostaining. (H) Fluorescence images of monolayers showing EDU staining (green, at day 3), Sox9 (green, at day3), Muc2 (red, at day 6), ChgA (red, at day 6), β-catenin (red, at day 6), actin (green), and integrin-β4 (red, at day 6) immunostaining. In all images Hoechst 33342 (blue) marked the nuclei.

stained for proliferative (EDU) and differentiated cells (absorptive colonocytes and goblet) (Figure 6C). Quantitative image analysis of the fluorescence intensities for lineage readouts was used to compare monolayers exposed to the compounds and the control monolayers that lacked exposure to the compounds. Differences between the dietary compounds and negative controls were assessed by using the SSMD, a commonly used statistic to identify potential hits in a library screen.[26] SSMD is a measure of the average fold change between a test compound and a negative reference, penalized by the variability of the fold change.

Prior reports in a variety of experimental systems indirectly corroborate the data obtained from the 2-D monolayers of primary murine cells. Multiple compounds (19 of 77, 25%) were growth suppressive, reducing the Hoechst-stained area (eg, cell number) relative to that of the control cells with fairly strong or stronger SSMD effect sizes (Figure 6A, B, and D; Supplementary Figure 1). For example, compounds identified as growth suppressive for the primary cells, eg, many of the fatty acids, nitrates, terpenoids, and curcuminoids, are all known to either promote differentiation or exhibit cell toxicity.[38,39] Glucoraphanin (#70), responsible for the bitterness of cabbage and Brussels

sprouts, reduced epithelial cell numbers to near 0, consistent with its reported toxicity when consumed in large amounts. Enterolactone (#75, a microbial metabolite of flaxseed) increased cell numbers relative to that of the control, consistent with its failure to prevent intestinal adenoma formation and pose an increased cancer risk when at very high levels.[40] A number of other compounds, such as the phenols gallic acid (#28) and ellagic acid (#29), suppressed the number of cells in S-phase without reducing the number of nuclei. Other molecules such as valproate (#6) and β-carotene (#58) display a similar growth suppressive effect and are recognized in the literature as inducing cell differentiation.[41,42] Only 9 of 77 compounds (12%) demonstrated increased cell numbers relative to that of the control, with fairly strong or stronger SSMD effect sizes. A single compound, isorhamnetin (#21, a component of ginkgo biloba), greatly increased cell numbers in S-phase. Ginkgo biloba is known to increase cell division in neurons and appears to have a similar impact on primary colonic epithelial cells. Nontoxic compounds that decrease or increase colonic epithelial cell proliferation may be useful as cancer chemopreventatives or in intestinal repair after insult.
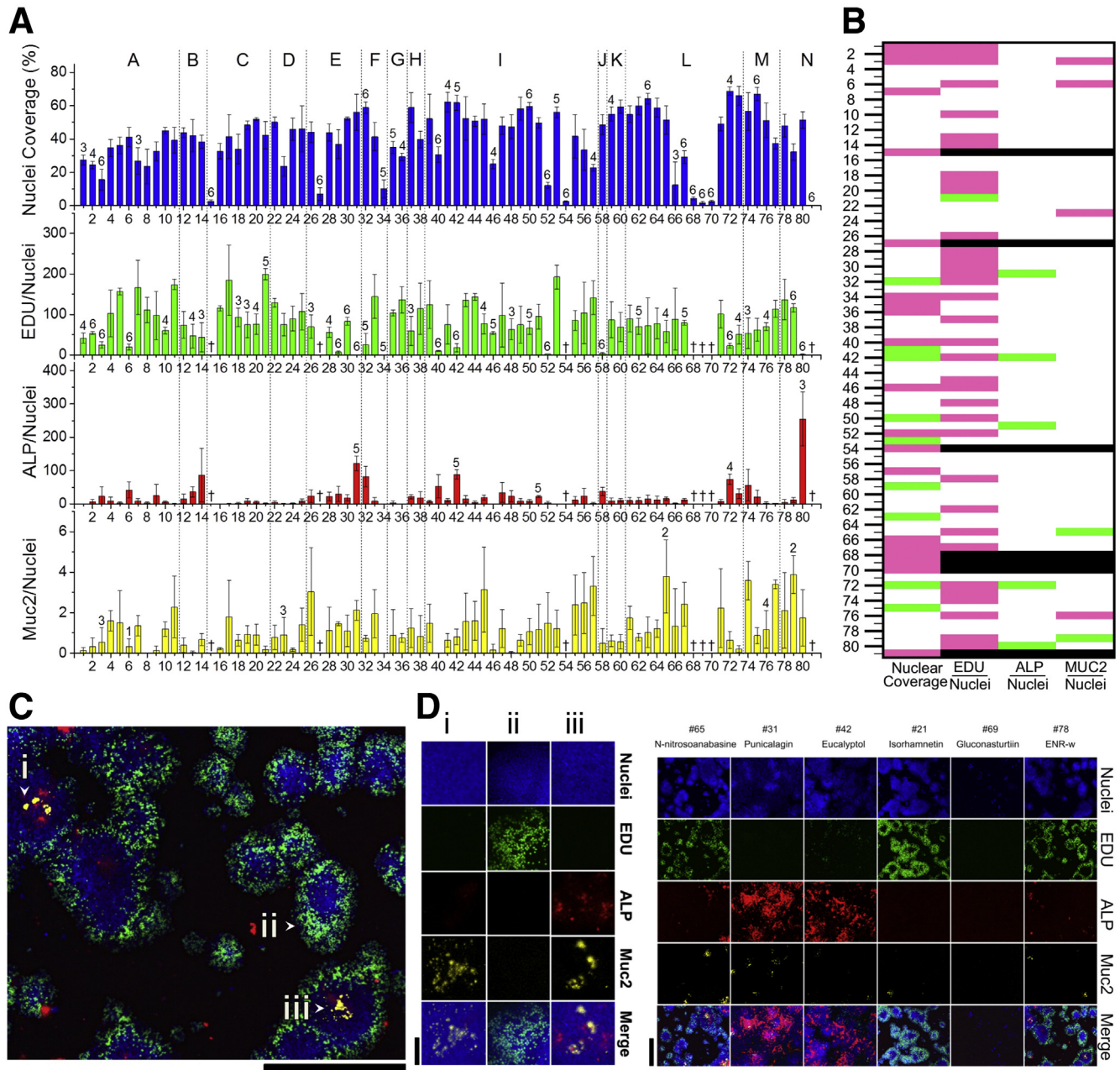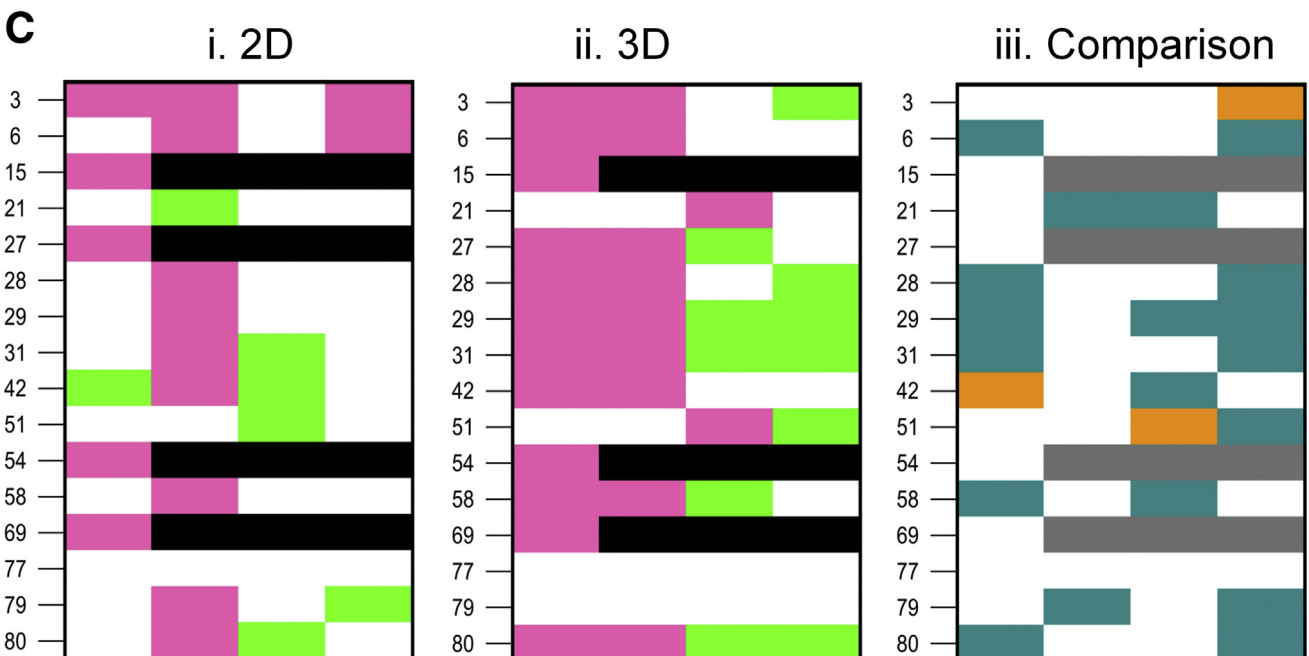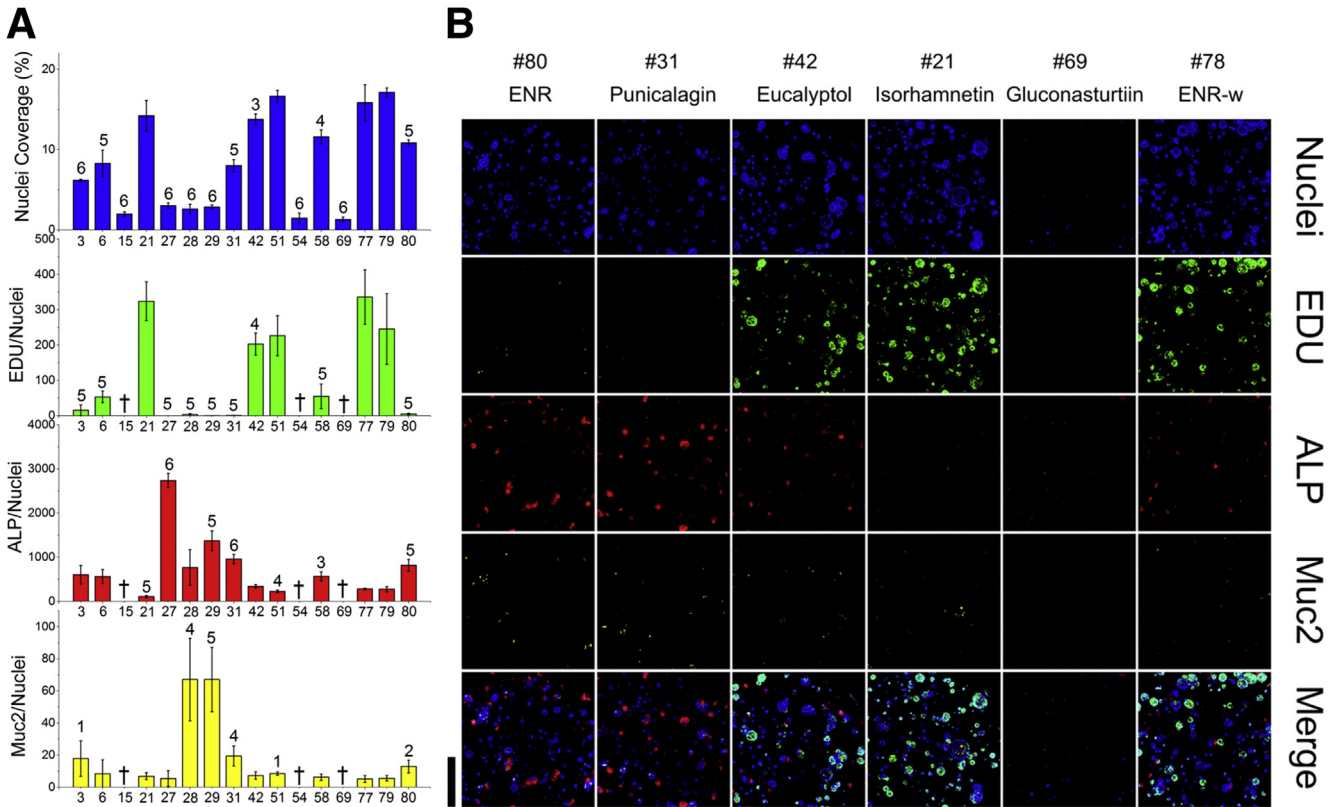
Figure 6. Impact of dietary compounds and natural products on primary murine colonic monolayers. (A) Percentage of collagen surface area that was positive for Hoechst 33342 and normalized fluorescence intensity due to EDU incorporation, ALP activity, or Muc2 staining was plotted against the compound number. EDU, ALP, and Muc2 fluorescence signals were normalized by summing the fluorescence intensity and dividing by nuclear percent area (ie, an indicator of cell number). Hits were designated as 6, extremely strong; 5, very strong; 4, strong; 3, fairly strong; 2, moderate; 1, fairly moderate (Moderate and fairly moderate effects were designated only for compounds within the Muc2 screen). †Cultures with extensive cell death (≤10% nuclear coverage). Bars represent the average, and error bar is a single standard deviation. (B) Map of hit compounds. *Green* and *pink* indicate an increased or decreased value, respectively, relative to that of the control (ENR-w). *Black* indicates cultures with extensive cell death. (C) Views of raw fluorescence images from screened primary mouse colonic epithelium. (*Left*) Full-well composite fluorescence image of primary mouse colonic epithelium in control ENR-w medium. Scale bar = 1 mm. (*Right*) Fluorescence images of colony regions with "*i*" marking ALP+ and Muc2+ cells, "*ii*" marking EDU+ cells, and "*iii*" denoting Muc2+ cells. Scale bar = 100 μm. (D) Representative fluorescence images from the compound screen. Scale bar = 1 mm.

Dietary metabolites or natural products directing cells into the differentiated colonic lineages are of profound interest for health maintenance and therapeutics. Although these effects are difficult to extrapolate from data on screens of other cell types or tumor cells, the ability of molecules to promote enterocyte or goblet-cell features was readily evaluated by using the 2-D murine monolayers. Four of the 77 molecules (5%) (eucalyptol,

#42; punicalagin, #31; phytol, #51; indole-3-butyric acid, #72) directed cells toward the absorptive colonocyte lineage as indicated by substantially increased ALP activity (Figure 5C). Eucalyptol (#42, used in flavorings, fragrances, and cosmetics) and punicalagin (#31, an antioxidant found in pomegranates) pushed murine cells toward the enterocyte lineage reported to block cell

proliferation, but by an unknown mechanism.[43] Other compounds (phytol, #51, a nuclear-receptor ligand used in the fragrance industry) directed murine cells toward the enterocyte lineage but did not reduce cell proliferation, suggesting a different or multiple modes of action relative to eucalyptol and punicalagin. A single compound, N-nitrosoanabasine (#65), increased Muc2 expression

with a moderate effect size (Figure 6D). These findings demonstrate the potential of this 2-D format as a high-content screening system to assay the impact of dietary compounds and microbial metabolites on intestinal health and disease.

To demonstrate the utility of 2-D cultures over 3-D cultures for enhanced compound screening, 14 compounds yielding significant alteration in proliferation or differentiation of the murine 2-D colonic cells were also assayed for their impact on the 3-D murine organoids (Figure 7A and B). The compounds were added to the 3-D organoids embedded in Matrigel and then assayed in a manner similar to that for the monolayer. The general response of the organoids to many of the compounds was similar to that of the 2-D monolayer (Figure 7C). However, compound assay on the 3-D organoids was significantly more complex relative to that on the monolayers, and this may account for many of the differences that were observed. The organoids existed in multiple image planes and underwent uncontrolled shape and size changes during the fixation/staining process, making quantification of fluorescence, area, and volume challenging. The surface area occupied by the Hoechst stain in the monolayers acted as an easily quantifiable and reliable surrogate for cell number in the 2-D monolayers; however, for the reasons stated above, this metric was not possible with the 3-D organoids when using conventional microscopy. The inability to use a simple metric such as Hoechst fluorescence surface area or intensity to track changes in cell number highlights the challenges for high-throughput compound screens using 3D organoids. Staining for ALP and Mucin2 was a simple process in the 2-D monolayers, with staining reagents added to the luminal monolayer surface where these molecules reside. In contrast, reagents added to the 3-D organoids must diffuse through a hydrogel and cell layer to access the luminal epithelium of the organoid. For example, we observed that fragmented or burst organoids stained more intensely for ALP (located at the luminal cell surface) relative to intact organoids in response to the same compound. Tannic acid (#27) significantly reduced cell growth in the 2-D monolayers but not in the 3-D organoids. This may be due to the different cell surfaces (luminal side in 2-D and basal side in 3-D) to which the compound was added. Tannic acid's lack of membrane permeability may have prevented exposure of the luminal organoid surface to this molecule. This comparison between the monolayers and organoids demonstrates the fundamental differences in the 2 systems as well as the significant advantages of the monolayers in screening applications.

Screening Dietary Metabolites and Natural Products on Human Tumor Cell Lines and Primary Human Rectal Cells

Tumor-derived Caco-2 cells have been adopted by pharmaceutical and biotechnology companies as the industry standard for drug screening in the intestine. To determine whether there are different responses of Caco-2 cells and the 2-D primary tissue-derived monolayers, the impact of 7 of the screened compounds on Caco-2 monolayers was assayed and compared with the results obtained from primary human monolayers. The tumor cells were cultured in their standard medium and human primary cells were cultured in HISC for 24 hours, followed by addition of the library compounds. After 48 hours, the primary human and Caco-2 cells were stained and evaluated for cell number, proliferation, absorptive cell phenotype, and goblet cell attributes as described for murine 2-D cultures (Figure 8B and c). At least 50% of the measurements trended in the opposite direction when the response of the 2 cell types to the compounds was measured (Figure 8A). For example, valproate (#6) decreased nuclear coverage and increased ALP expression in Caco-2 cells but generated the opposite responses in the primary cells. Thus, valproate may direct Caco-2 cells but not primary cells into the absorptive cell lineage under these conditions. Punicalagin (#31) strongly reduced EDU incorporation in the primary cells but generated the opposite effect in the Caco-2 cells. Punicalagin slows the growth of primary cells but may encourage proliferation in the tumor cells. These data demonstrate distinct differences between the Caco-2 tumor cells and the 2-D primary monolayer for a number of compounds, suggesting that tumor cells might respond differently to dietary compounds than primary cells. A larger compound screen would likely reveal a greater number of discrepancies between the 2 cell types. Nevertheless, these data demonstrate that the human monolayers are suitable for compound screening in a manner similar to the murine monolayers.

Figure 7. (*See previous page*). **Assaying a subset of dietary compounds and metabolites on murine 3-D organoids.** (*A*) Percentage of collagen surface area that was positive for Hoechst 33342 and normalized fluorescence intensity due to EDU incorporation, ALP activity, or Muc2 staining was plotted against the compound number. EDU, ALP, and Muc2 fluorescence signals were normalized by summing the fluorescence intensity and dividing by nuclear percent area (ie, an indicator of cell number). Hits were designated as subtypes: 6, extremely strong; 5, very strong; 4, strong; 3, fairly strong; 2, moderate; 1, fairly moderate (Moderate and fairly moderate effects were designated only for compounds within the Muc2 screen). †Cultures with extensive cell death (≤10% nuclear coverage for 2-D or ≤2% nuclear coverage for 3-D). Bars represent the average, and error bar is a single standard deviation. (*B*) Representative fluorescence images from the assay. Scale bar = 1 mm. (*C*) (*i*) and (*ii*) Comparison of effect of selected compounds on 2-D monolayer and 3-D organoids. *Green* and *pink* indicate increased or decreased value, respectively, relative to that of the control (ENR-w). *Black* indicates cultures with extensive cell death. (*iii*) Direct comparison of responses of 2-D monolayers and 3-D organoids to the compounds. *White* indicates strong response by both cultures in same direction (enhanced or diminished effect) or weak response by both cultures. *Green-blue* indicates strong response in one culture system but not the other. *Orange* indicates strong responses in both cultures but in opposite directions. *Grey* indicates that no comparison of the 2 cell types was made.
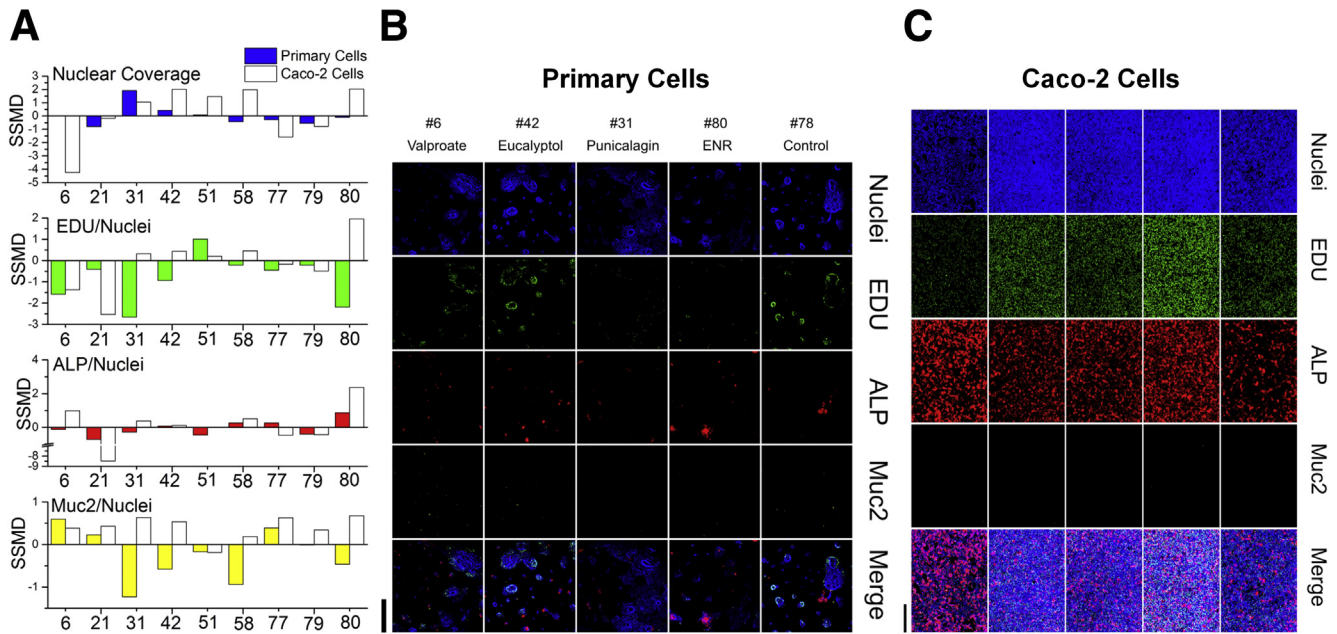
Figure 8. Impact of 7 dietary compounds and natural products on human primary rectal and tumor Caco-2 cells. (*A*) SSMD effect size was plotted against the compound number for the 4 screen readouts: percentage of image surface area that was positive for Hoechst 33342 and the normalized fluorescence intensity due to EDU incorporation, ALP activity, or Muc2 staining. EDU, ALP, and Muc2 fluorescence signals were normalized by summing the fluorescence intensity and dividing by nuclear percent area (ie, indicator of cell number). |SSMD| > 1.645 is required to designate a strong effect size. (*B* and *C*) Representative fluorescence images from the assays. Control medium for Caco-2 cells was Dulbecco modified Eagle medium. Scale bar = 1 mm.

Conclusions

Studies using 3-D colonic organoids have provided novel insights into intestinal biology; however, the enclosed organoid architecture possesses severe limitations in screening applications and for many basic biomedical investigations. The organoid lumen buried within a hydrogel is inaccessible to drugs, toxins, probiotics, microbiota, and other agents in contrast to the gut lumen of a living animal. We developed a self-renewing, 2-D monolayer derived from primary intestinal tissue and possessing all cell lineages found within the colon. Long-term cell proliferation on the collagen hydrogel was likely due to its similar chemical makeup and stiffness relative to those of the basement membrane underlining the colonic epithelium. Cells of the organoids expand at a slower rate than those of the monolayer, potentially as a result of the added requirement of the hydrogel-embedded cells to remove and remodel the matrix during expansion. Remarkably, the monolayers self-pattern to create peripheral stem/proliferative and central differentiated cell zones. The interior of the monolayer yields a large surface area occupied predominantly by differentiated cells, a feature mimicking that of the intestinal surface area in vivo. Importantly, the chemical environment of the monolayer is readily manipulated by addition of compounds to the media overlying the cells. This programmable feature in combination with the open architecture and accessible luminal face enables facile assay of drugs, toxins, and metabolites not possible in the organoid systems. Standard high-content microscopy methods were readily paired with the 2-D monolayers to identify the impact of dietary metabolites and natural products on primary intestinal cells obtained directly from animal models.

References

1. Grossmann J, Walther K, Artinger M, et al. Progress on isolation and short-term ex-vivo culture of highly purified non-apoptotic human intestinal epithelial cells (IEC). Eur J Cell Biol 2003;82:262–270.

2. Engle MJ, Goetz GS, Alpers DH. Caco-2 cells express a combination of colonocyte and enterocyte phenotypes. J Cell Physiol 1998;174:362–369.

3. Sun H, Chow ECY, Liu S, et al. The Caco-2 cell monolayer: usefulness and limitations. Expert Opin Drug Metab Toxicol 2008;4:395–411.

4. Ahmad AA, Wang YL, Gracz AD, et al. Optimization of 3-D organotypic primary colonic cultures for organ-on-chip applications. J Biol Eng 2014;8:9.

5. Jung P, Sato T, Merlos-Suarez A, et al. Isolation and in vitro expansion of human colonic stem cells. Nat Med 2011;17:1225–1227.

6. Sato T, Clevers H. Growing self-organizing mini-guts from a single intestinal stem cell: mechanism and applications. Science 2013;340:1190–1194.

7. Sato T, Stange DE, Ferrante M, et al. Long-term expansion of epithelial organoids from human colon, adenoma, adenocarcinoma, and Barrett's epithelium. Gastroenterology 2011;141:1762–1772.

8. Sato T, Vries RG, Snippert HJ, et al. Single Lgr5 stem cells build crypt-villus structures in vitro without a mesenchymal niche. Nature 2009;459:262–265.

9. Aoki R, Shoshkes-Carmel M, Gao N, et al. Foxl1-expressing mesenchymal cells constitute the intestinal stem cell niche. Cell Mol Gastroenterol Hepatol; 2:175–188.

10. Kieckhaefer JE, Lukovac S, Ye DZ, et al. The RNA polymerase III subunit Polr3b is required for the maintenance of small intestinal crypts in mice. Cell Mol Gastroenterol Hepatol 2016;2:783–795.

11. Clevers H. Modeling development and disease with organoids. Cell 2016;165:1586–1597.

12. Zachos NC, Kovbasnjuk O, Foulke-Abel J, et al. Human enteroids/colonoids and intestinal organoids functionally recapitulate normal intestinal physiology and pathophysiology. J Biol Chem 2016;291:3759–3766.

13. Astashkina A, Mann B, Grainger DW. A critical evaluation of in vitro cell culture models for high-throughput drug screening and toxicity. Pharmacol Ther 2012; 134:82–106.

14. Randall KJ, Turton J, Foster JR. Explant culture of gastrointestinal tissue: a review of methods and applications. Cell Biol Toxicol 2011;27:267–284.

15. Seidelin JB, Horn T, Nielsen OH. Simple and efficient method for isolation and cultivation of endoscopically obtained human colonocytes. Am J Physiol Gastrointest Liver Physiol 2003;285:G1122–G1128.

16. Moon C, VanDussen KL, Miyoshi H, et al. Development of a primary mouse intestinal epithelial cell monolayer culture system to evaluate factors that modulate IgA transcytosis. Mucosal Immunol 2014;7:818–828.

17. In J, Foulke-Abel J, Zachos NC, et al. Enterohemorrhagic Escherichia coli reduces mucus and intermicrovillar bridges in human stem cell-derived colonoids. Cell Mol Gastroenterol Hepatol 2016;2:48–62.

18. Snippert HJ, van der Flier LG, Sato T, et al. Intestinal crypt homeostasis results from neutral competition between symmetrically dividing Lgr5 stem cells. Cell 2010;143:134–144.

19. Wang Y, Ahmad AA, Shah PK, et al. Capture and 3D culture of colonic crypts and colonoids in a microarray platform. Lab on a Chip 2013;13:4625–4634.

20. Miyoshi H, Stappenbeck TS. In vitro expansion and genetic modification of gastrointestinal stem cells in spheroid culture. Nat Protoc 2013;8:2471–2482.

21. Paguirigan AL, Beebe DJ. Protocol for the fabrication of enzymatically crosslinked gelatin microchannels for microfluidic cell culture. Nat Protoc 2007;2:1782–1788.

22. Salic A, Mitchison TJ. A chemical method for fast and sensitive detection of DNA synthesis in vivo. Proc Natl Acad Sci U S A 2008;105:2415–2420.

23. Ramalingam S, Daughtridge GW, Johnston MJ, et al. Distinct levels of Sox9 expression mark colon epithelial stem cells that form colonoids in culture. Am J Physiol Gastrointest Liver Physiol 2012;302:G10–G20.

24. Wang YL, Ahmad AA, Sims CE, et al. In vitro generation of colonic epithelium from primary cells guided by microstructures. Lab on a Chip 2014;14: 1622–1631.

25. Wong VW, Stange DE, Page ME, et al. Lrig1 controls intestinal stem-cell homeostasis by negative regulation of ErbB signalling. Nat Cell Biol 2012;14:401–408.

26. Zhang XD. A new method with flexible and balanced control of false negatives and false positives for hit selection in RNA interference high-throughput screening assays. J Biomol Screen 2007;12:645–655.

27. Zhang XD. A method for effectively comparing gene effects in multiple conditions in RNAi and expression-profiling research. Pharmacogenomics 2009;10:345–358.

28. Zhang XHD. Illustration of SSMD, z score, SSMD*, z* score, and t statistic for hit selection in RNAi high-throughput screens. J Biomol Screen 2011;16: 775–785.

29. Lai YZ, Asthana A, Kisaalita WS. Biomarkers for simplifying HTS 3D cell culture platforms for drug discovery: the case for cytokines. Drug Discov Today 2011; 16:293–297.

30. Ali MY, Chuang CY, Saif MTA. Reprogramming cellular phenotype by soft collagen gels. Soft Matter 2014; 10:8829–8837.

31. Curtis ASG, Forrester JV, McInnes C, et al. Adhesion of cells to polystyrene surfaces. J Cell Physiol 1983; 97:1500–1506.

32. Leclerc E, Sakai Y, Fujii T. Cell culture in 3-dimensional microfluidic structure of PDMS (polydimethylsiloxane). Biomed Microdevices 2003;5:109–114.

33. Fuard D, Tzvetkova-Chevolleau T, Decossas S, et al. Optimization of poly-di-methyl-siloxane (PDMS) substrates for studying cellular adhesion and motility. Microelectron Eng 2008;85:1289–1293.

34. Wypych G. Handbook of polymers. Toronto: ChemTec Publishing, 2012.

35. Yang J, Nandi S. Growth of cultured cells using collagen as substrate. International Review of Cytology: a Survey of Cell Biology 1983;81:249–286.

36. Gracz AD, Ramalingam S, Magness ST. Sox9 expression marks a subset of CD24-expressing small intestine epithelial stem cells that form organoids in vitro. Am J Physiol Gastrointest Liver Physiol 2010;298: G590–G600.

37. Blache P, van de Wetering M, Duluc I, et al. SOX9 is an intestine crypt transcription factor, is regulated by the Wnt pathway, and represses the CDX2 and MUC2 genes. J Cell Physiol 2004;166:37–47.

38. Hebels DG, Brauers KJ, van Herwijnen MH, et al. Time-series analysis of gene expression profiles induced by nitrosamides and nitrosamines elucidates modes of action underlying their genotoxicity in human colon cells. Toxicol Lett 2011;207:232–241.

39. Johnson IT. Anticarcinogenic effects of diet-related apoptosis in the colorectal mucosa. Food Chem Toxicol 2002;40:1171–1178.

40. Oikarinen SI, Pajari AM, Salminen I, et al. Effects of a flaxseed mixture and plant oils rich in alpha-linolenic acid on the adenoma formation in multiple intestinal neoplasia (Min) mice. Br J Nutr 2005;94:510–518.

41. Handelman GJ. The evolving role of carotenoids in human biochemistry. Nutrition 2001;17:818–822.

42. Teng CL, Han SM, Wu WC, et al. Mechanistic aspects of lauryl gallate-induced differentiation and apoptosis in human acute myeloid leukemia cells. Food Chem Toxicol 2014;71:197–206.

43. Bayala B, Bassole IH, Gnoula C, et al. Chemical composition, antioxidant, anti-inflammatory and anti-proliferative activities of essential oils of plants from Burkina Faso. PLoS One 2014;9:e92122.

Supplementary Figure 1. Descending plots showing impact of dietary compounds and natural products on primary mouse colonic epithelium. Percentage of collagen surface area that demonstrated fluorescence due to Hoechst 33342, EDU incorporation, ALP activity, or Muc2 staining was plotted against the compound number indicated on the x-axis. EDU, ALP, and Muc2 areas were normalized to the nuclear area. Compounds were ranked by their SSMD effect sizes, and hits were selected from compounds exceeding SSMD thresholds. Hits were designated as effect subtypes: 6, extremely strong; 5, very strong; 4, strong; 3, fairly strong; 2, moderate; 1, fairly moderate (Moderate and fairly moderate effects were designated only for compounds within the Muc2 screen). †Cultures with extensive cell death ($\leq$10% nuclear coverage); *Control medium; **Control differentiation medium.

Supplementary Table 1. Composition of Media Used in This Study[1]

Reagent name	Source	Mouse medium abbreviation		Human medium
		ENR-W	ENR-w	HISC
Wnt-3A	Conditioned medium	30 ng/mL	10 ng/mL	100 ng/mL
R-spondin 2	Conditioned medium	75 ng/mL	75 ng/mL	90 ng/mL
Noggin	Conditioned medium	71 ng/mL	71 ng/mL	43 ng/mL
EGF	Peprotech	50 ng/mL	50 ng/mL	50 ng/mL
n-Acetylcysteine	MP Bio	1 mmol/L	1 mmol/L	1.25 mmol/L
HEPES	Life Technologies	10 mmol/L	10 mmol/L	10 mmol/L
Gentamicin	Life Technologies	5 μg/mL	5 μg/mL	5 μg/mL
A-8301	Sigma-Aldrich	500 nmol/L	500 nmol/L	500 nmol/L[a]
B27	Life Technologies			×1
Nicotinamide	Sigma-Aldrich			10 mmol/L
Gastrin	AnaSpec			10 nmol/L
SB202190	Sigma-Aldrich			3 μmol/L
Prostaglandin E$_2$	Cayman Chemicals			10 nmol/L
Y-27632	ApexBio	10 μmol/L[b]	10 μmol/L[b]	10 μmol/L[b]

[a]A-8301, a transforming growth factor-beta inhibitor, was observed to inhibit spreading of human rectal epithelial cells as 2-D monolayer, so it was not included for the first 48 hours after plating of human cells.
[b]Used in the first 48 hours after cell plating to prevent dissociation-induced cell apoptosis.

Supplementary Table 2. List of Dietary Compounds and Natural Products and Their Working Concentration for the Study

No.	Category 1	Category 2	Compound name	Concentration for study (mmol/L)
1	Fatty acids	Short-chain fatty acids	Acetate[2]	24
2			Butyrate[3]	1
3			Propionate[2]	6
4			3-Hydroxybutyrate[4]	5
5			Formate[5]	10
6			Valproate[1]	2
7		Medium-chain fatty acids	Capric acid/decanoic acid[6]	0.1
8		Long-chain fatty acids	Docosahexanoic acid[7]	0.1
9		Other acids	Nicotinic acid[8]	5
10			Succinic acid[9]	2
11			Pamoic acid[10]	0.001
12	Secondary bile acids		Deoxycholic acid[11]	0.001
13			Ursodeoxycholic acid[12]	0.188
14			Hyodeoxycholic acid[12]	0.188
15	Flavonoids		Luteolin[13]	0.25
16			Tangeritin[14]	0.05
17			Quercetin[15]	0.05
18			Kaempferol[16]	0.06
19			Myricetin[17]	0.04
20			Fisetin[18]	0.01
21			Isorhamnetin[19]	0.05
22	Phytoestrogens		Daidzin[20]	0.02
23			Genistin[21]	0.03
24			Daiszein (a glycone of daidzen)[22]	0.05
25			Genistein (a glycine of genistin)[23]	0.015
26	Phenols		Carbolic acid (phenol)	0.034
27			Tannic acid[24]	0.034
28			Gallic acid[25]	0.02
29			Ellagic acid[26]	0.06
30			Chlorogenic acid[26]	0.06
31			Punicalagin[27]	0.01
32	Stilbenes		Aglycones (staurosporine)[28]	0.0003
33			Pinosylvin[29]	0.001
34			Resveratrol[29]	0.1
35	Curcuminoids		Bisdemethoxycurcumin[30]	0.034
36			Demethoxycurcumin[30]	0.034
37	Chalconoids		Dihydrochalcone[31]	0.034
38			Chalcone[32]	0.02
39	Terpenoids		Isoprene[33]	5
40			Isovaleric acid[34]	10
41			Geranyl pyrophosphate[35]	0.015
42			Eucalyptol[36]	1
43			R-Limonene[37]	1
44			Pinene[38]	0.3
45			Farnesyl pyrophosphate[35]	0.015
46			Artemisinin[39]	0.1
47			Bisabolol[40]	0.005
48			Geranylgeranyl pyrophosphate[41]	0.005
49			Retinol[42]	0.001
50			Retinal[43]	0.000001
51			Phytol[44]	0.2
52			Taxol (paclitaxel)[45]	0.02
53			Forskolin[46]	0.005
54			Aphidicolin[47]	0.06
55			Salvinorin[48]	0.001
56			Squalene[49]	0.05
57			Lanosterol[50]	0.04
58	Carotenoids		β-carotene[51]	5
59	Phytosterols		β-sitosterol[52]	0.13
60			Campesterol[53]	0.006

Supplementary Table 2. Continued

No.	Category 1	Category 2	Compound name	Concentration for study (mmol/L)
61	Nitrates	Nitrosamines	N-nitrosonornicotine[54]	0.001
62			4-(methylnitrosamino)-1-(3-pyridyl)-1-butanone[55]	0.01
63			N-nitrosodimethylamine[56]	0.05
64			N-nitrodiethylamine[57]	2
65			N-nitrosoanabasine[58]	0.989
66		Nitrosoguanidine	N-methyl-N-nitroso-p-toluenesulfonamide	0.989
67		Glucosinolates	Sinigrin[59]	0.989
68			Glucotropaeolin isothiocyanate[60]	6
69			Gluconasturtiin[61]	0.1
70			Glucoraphanin[62]	1
71		Indoles	Indole[63]	0.675
72			Indole-3-butyric acid[64]	0.058
73			3-Methylindole[65]	0.000005
74	Plant lignins		Enterodiol[66]	0.01
75			Enterolactone[66]	0.01
76			Secoisolariciresinol[67]	0.1
77			Matairesinol[68]	0.05
78	Control	ENR-w medium	Containing 10 ng/mL Wnt-3A and 1/1000 water	
79		ENR-w + DMSO	Containing 10 ng/mL Wnt-3A and 1/1000 DMSO	
80		ENR	Differentiation medium	
81		No cells	Collagen hydrogel	

NOTE. For primary cells, all media were based on ENR-w media that contained 10 ng/mL Wnt-3A. For Caco-2 cells, all media except #80 were based on Dulbecco modified Eagle medium (DMEM). Caco-2 controls were as follows: #78 is DMEM medium; #79 is DMEM medium with 1/1000 DMSO; #80 is ENR medium; and #81 is DMEM medium without cells. DMSO, dimethyl sulfoxide.

Supplementary References

1. Yin XL, Farin HF, van Es JH, et al. Niche-independent high-purity cultures of Lgr5(+) intestinal stem cells and their progeny. Nat Methods 2014;11:106–112.

2. Comalada M, Bailon E, de Haro O, et al. The effects of short-chain fatty acids on colon epithelial proliferation and survival depend on the cellular phenotype. J Cancer Res Clin Oncol 2006;132:487–497.

3. Kaiko GE, Ryu SH, Koues OI, et al. The colonic crypt protects stem cells from microbiota-derived metabolites. Cell 2016;165:1708–1720.

4. Ooi CC, Good NM, Williams DB, et al. Structure-activity relationship of butyrate analogues on apoptosis, proliferation and histone deacetylase activity in HCT-116 human colorectal cancer cells. Clin Exp Pharmacol Physiol 2010;37:905–911.

5. Malago JJ, Koninkx J, Douma PM, et al. Differential modulation of enterocyte-like Caco-2 cells after exposure to short-chain fatty acids. Food Additives and Contaminants 2003;20:427–437.

6. Chao AC, Nguyen JV, Broughall M, et al. In vitro and in vivo evaluation of effects of sodium caprate on enteral peptide absorption and on mucosal morphology. Int J Pharm 1999;191:15–24.

7. Usami M, Komurasaki T, Hanada A, et al. Effect of gamma-linolenic acid or docosahexaenoic acid on tight junction permeability in intestinal monolayer cells and their mechanism by protein kinase C activation and/or eicosanoid formation. Nutrition 2003;19:150–156.

8. Haas MJ, Alamir AR, Sultan S, et al. Nicotinic acid induces apolipoprotein A-I gene expression in HepG2 and Caco-2 cell lines. Metabolism-Clinical and Experimental 2011;60:1790–1796.

9. Salovaara S, Sandberg AS, Andlid T. Organic acids influence iron uptake in the human epithelial cell line Caco-2. J Agric Food Chem 2002;50:6233–6238.

10. Zhao PW, Sharir H, Kapur A, et al. Targeting of the orphan receptor GPR35 by pamoic acid: a potent activator of extracellular signal-regulated kinase and beta-arrestin2 with antinociceptive activity. Mol Pharmacol 2010;78:560–568.

11. Ridlon JM, Bajaj JS. The human gut sterolbiome: bile acid-microbiome endocrine aspects and therapeutics. Acta Pharm Sin B 2015;5:99–105.

12. Araki Y, Fujiyama Y, Andoh A, et al. Hydrophilic and hydrophobic bile acids exhibit different cytotoxicities through cytolysis, interleukin-8 synthesis and apoptosis in the intestinal epithelial cell lines: IEC-6 and Caco-2 cells. Scand J Gastroenterol 2001;36:533–539.

13. Abbasi N, Akhavan MM, Rahbar-Roshandel N, et al. The effects of low and high concentrations of luteolin on cultured human endothelial cells under normal and glucotoxic conditions: involvement of integrin-linked kinase and cyclooxygenase-2. Phytother Res 2014;28:1301–1307.

14. Cheng Z, Surichan S, Ruparelia K, et al. Tangeretin and its metabolite 4'-hydroxytetramethoxyflavone attenuate EGF-stimulated cell cycle progression in hepatocytes: role of inhibition at the level of mTOR/p70S6K. Br J Pharmacol 2011;162:1781–1791.

15. Refolo MG, D'Alessandro R, Malerba N, et al. Anti proliferative and pro apoptotic effects of flavonoid quercetin are mediated by CB1 receptor in human colon cancer cell lines. J Cell Physiol 2015;230:2973–2980.

16. Moskot M, Jakobkiewicz-Banecka J, Smolinska E, et al. Activities of genes controlling sphingolipid metabolism in human fibroblasts treated with flavonoids. Metab Brain Dis 2015;30:1257–1267.

17. Huang H, Chen AY, Rojanasakul Y, et al. Dietary compounds galangin and myricetin suppress ovarian cancer cell angiogenesis. J Funct Foods 2015;15:464–475.

18. Mukhtar E, Adhami VM, Sechi M, et al. Dietary flavonoid fisetin binds to beta-tubulin and disrupts microtubule dynamics in prostate cancer cells. Cancer Lett 2015;367:173–183.

19. Duan J, Xie Y, Luo H, et al. Transport characteristics of isorhamnetin across intestinal Caco-2 cell monolayers and the effects of transporters on it. Food Chem Toxicol 2014;66:313–320.

20. Keung WM, Vallee BL. Daidzin: a potent, selective inhibitor of human mitochondrial aldehyde dehydrogenase. Proc Natl Acad Sci U S A 1993;90:1247–1251.

21. Kopečná-Zapletalová M, Krasulová K, Anzenbacher P, et al. Interaction of isoflavonoids with human liver microsomal cytochromes P450: inhibition of CYP enzyme activities. Xenobiotica 2016:1–8.

22. Toro-Funes N, Morales-Gutierrez FJ, Veciana-Nogues MT, et al. The intracellular metabolism of isoflavones in endothelial cells. Food Funct 2015;6:98–108.

23. Donovan SM, Andres A, Mathai RA, et al. Soy formula and isoflavones and the developing intestine. Nutr Rev 2009;67(Suppl 2):S192–S200.

24. Druzhyna N, Szczesny B, Olah G, et al. Screening of a composite library of clinically used drugs and well-characterized pharmacological compounds for cystathionine β-synthase inhibition identifies benserazide as a drug potentially suitable for repurposing for the experimental therapy of colon cancer. Pharmacol Res 2016;113(Part A):18–37.

25. Lu Z, Nie G, Belton PS, et al. Structure–activity relationship analysis of antioxidant ability and neuroprotective effect of gallic acid derivatives. Neurochem Int 2006;48:263–274.

26. Das M, Bickers DR, Mukhtar H. Plant phenols as in vitro inhibitors of glutathione S-transferase(s). Biochem Biophys Res Commun 1984;120:427–433.

27. Lee SI, Kim BS, Kim KS, et al. Immune-suppressive activity of punicalagin via inhibition of NFAT activation. Biochem Biophys Res Commun 2008;371:799–803.

28. Thompson AF, Levin LA. Neuronal differentiation by analogs of staurosporine. Neurochem Int 2010;56:554–560.

29. Perecko T, Drabikova K, Nosal R, et al. Involvement of caspase-3 in stilbene derivatives induced apoptosis of human neutrophils in vitro. Interdiscip Toxicol 2012;5:76–80.

30. Yang H, Fan S, An Y, et al. Bisdemethoxycurcumin exerts pro-apoptotic effects in human pancreatic adenocarcinoma cells through mitochondrial dysfunction and a GRP78-dependent pathway. Oncotarget 2016;7:83641–83656.

31. Hu L, Li L, Xu D, et al. Protective effects of neohesperidin dihydrochalcone against carbon tetrachloride-induced oxidative damage in vivo and in vitro. Chem Biol Interact 2014;213:51–59.

32. Hachet-Haas M, Balabanian K, Rohmer F, et al. Small neutralizing molecules to inhibit actions of the chemokine CXCL12. J Biol Chem 2008;283:23189–23199.

33. Fabiani R, Rosignoli P, De Bartolomeo A, et al. DNA-damaging ability of isoprene and isoprene mono-epoxide (EPOX I) in human cells evaluated with the comet assay. Mutat Res 2007;629:7–13.

34. Sakurazawa T, Ohkusa T. Cytotoxicity of organic acids produced by anaerobic intestinal bacteria on cultured epithelial cells. J Gastroenterol 2005;40:600–609.

35. Gan X, Kaplan R, Menke JG, et al. Dual mechanisms of ABCA1 regulation by geranylgeranyl pyrophosphate. J Biol Chem 2001;276:48702–48708.

36. Zhang W, Lim LY. Effects of spice constituents on P-glycoprotein-mediated transport and CYP3A4-mediated metabolism in vitro. Drug Metab Dispos 2008;36:1283–1290.

37. Yoshida N, Takagi A, Kitazawa H, et al. Inhibition of P-glycoprotein-mediated transport by extracts of and monoterpenoids contained in Zanthoxyli fructus. Toxicol Appl Pharmacol 2005;209:167–173.

38. Jensen-Jarolim E, Gajdzik L, Haberl I, et al. Hot spices influence permeability of human intestinal epithelial monolayers. J Nutr 1998;128:577–581.

39. Augustijns P, D'Hulst A, Van Daele J, et al. Transport of artemisinin and sodium artesunate in Caco-2 intestinal epithelial cells. J Pharm Sci 1996;85:577–579.

40. Cavalieri E, Bergamini C, Mariotto S, et al. Involvement of mitochondrial permeability transition pore opening in alpha-bisabolol induced apoptosis. FEBS J 2009;276:3990–4000.

41. Agarwal B, Halmos B, Feoktistov AS, et al. Mechanism of lovastatin-induced apoptosis in intestinal epithelial cells. Carcinogenesis 2002;23:521–528.

42. Plateroti M, Sambuy Y, Nobili F, et al. Expression of epithelial markers and retinoid-binding proteins in retinol- or retinoic acid-treated intestinal cells in vitro. Exp Cell Res 1993;208:137–147.

43. Boskovic G, Twining SS. Retinol and retinaldehyde specifically increase alpha1-proteinase inhibitor in the human cornea. Biochem J 1997;322(Pt 3):751–756.

44. Lampen A, Meyer S, Nau H. Phytanic acid and docosahexaenoic acid increase the metabolism of all-trans-retinoic acid and CYP26 gene expression in intestinal cells. Biochim Biophys Acta 2001;1521:97–106.

45. Walle UK, Walle T. Taxol transport by human intestinal epithelial Caco-2 cells. Drug Metab Dispos 1998;26:343–346.

46. Dekkers JF, Wiegerinck CL, de Jonge HR, et al. A functional CFTR assay using primary cystic fibrosis intestinal organoids. Nat Med 2013;19:939–945.

47. DiGiuseppe JA, Hunting DJ, Dresler SL. Aphidicolin-sensitive DNA repair synthesis in human fibroblasts damaged with bleomycin is distinct from UV-induced repair. Carcinogenesis 1990;11:1021–1026.

48. Capasso R, Borrelli F, Capasso F, et al. The hallucinogenic herb Salvia divinorum and its active ingredient salvinorin A inhibit enteric cholinergic transmission in the guinea-pig ileum. Neurogastroenterol Motil 2006;18:69–75.

49. Warleta F, Campos M, Allouche Y, et al. Squalene protects against oxidative DNA damage in MCF10A human mammary epithelial cells but not in MCF7 and MDA-MB-231 human breast cancer cells. Food Chem Toxicol 2010;48:1092–1100.

50. Zhao L, Chen XJ, Zhu J, et al. Lanosterol reverses protein aggregation in cataracts. Nature 2015;523:607–611.

51. Ferruzzi MG, Lumpkin JL, Schwartz SJ, et al. Digestive stability, micellarization, and uptake of beta-carotene isomers by Caco-2 human intestinal cells. J Agric Food Chem 2006;54:2780–2785.

52. Baskar AA, Ignacimuthu S, Paulraj GM, et al. Chemopreventive potential of beta-Sitosterol in experimental colon cancer model: an in vitro and in vivo study. BMC Complement Altern Med 2010;10:24.

53. Fahy DM, O'Callaghan YC, O'Brien NM. Phytosterols: lack of cytotoxicity but interference with beta-carotene uptake in Caco-2 cells in culture. Food Addit Contam 2004;21:42–51.

54. Patten CJ, Smith TJ, Friesen MJ, et al. Evidence for cytochrome P450 2A6 and 3A4 as major catalysts for N'-nitrosonornicotine alpha-hydroxylation by human liver microsomes. Carcinogenesis 1997;18:1623–1630.

55. Smith TJ, Guo Z, Guengerich FP, et al. Metabolism of 4-(methylnitrosamino)-1-(3-pyridyl)-1-butanone (NNK) by human cytochrome P450 1A2 and its inhibition by phenethyl isothiocyanate. Carcinogenesis 1996;17:809–813.

56. Nowak A, Kuberski S, Libudzisz Z. Probiotic lactic acid bacteria detoxify N-nitrosodimethylamine. Food Addit Contam Part A Chem Anal Control Expo Risk Assess 2014;31:1678–1687.

57. Bansal AK, Bhatnagar D, Soni GL. In vitro effect of n-nitrosodiethylamine on lipid peroxidation and antioxidant system in human erythrocytes. Toxicol. Vitro 1996;10:649–653.

58. Liao J, Pan Y, Li C, et al. Fast screening for tobacco-specific N-nitrosamines by CZE using dynamically coated capillaries. Chromatographia 2011;74:415–419.

59. Weil MJ, Zhang Y, Nair MG. Colon cancer proliferating desulfosinigrin in wasabi (Wasabia japonica). Nutr Cancer 2004;48:207–213.

60. Combourieu B, Elfoul L, Delort AM, et al. Identification of new derivatives of sinigrin and glucotropaeolin produced by the human digestive microflora using 1H NMR spectroscopy analysis of in vitro incubations. Drug Metab Dispos 2001;29:1440–1445.

61. Natella F, Maldini M, Leoni G, et al. Glucosinolates redox activities: can they act as antioxidants? Food Chem 2014;149:226–232.

62. Luang-In V, Narbad A, Nueno-Palop C, et al. The metabolism of methylsulfinylalkyl- and methylthioalkyl-glucosinolates by a selection of human gut bacteria. Mol Nutr Food Res 2014;58:875–883.

63. Nikaido E, Giraud E, Baucheron S, et al. Effects of indole on drug resistance and virulence of Salmonella enterica

serovar Typhimurium revealed by genome-wide analyses. Gut Pathog 2012;4:5.

64. Beyaztaş S, Arslan O. Affinity to some plant growth regulators on human erythrocytes cytosolic carbonic anhydrase I and II. Hacettepe J Biol Chem 2009; 37:281–288.

65. Park YH, Shi YP, Liang B, et al. High-resolution metabolomics to discover potential parasite-specific biomarkers in a Plasmodium falciparum erythrocytic stage culture system. Malar J 2015;14:122.

66. Jansen GH, Arts IC, Nielen MW, et al. Uptake and metabolism of enterolactone and enterodiol by human colon epithelial cells. Arch Biochem Biophys 2005;435:74–82.

67. Mukker JK, Michel D, Muir AD, et al. Permeability and conjugative metabolism of flaxseed lignans by Caco-2 human intestinal cells. J Nat Prod 2014;77:29–34.

68. During A, Debouche C, Raas T, et al. Among plant lignans, pinoresinol has the strongest antiinflammatory properties in human intestinal Caco-2 cells. J Nutr 2012; 142:1798–1805.